

SPIRALS, BRIDGES, AND TAILS: A GALEX UV ATLAS OF INTERACTING GALAXIES

BEVERLY J. SMITH

Department of Physics and Astronomy, East Tennessee State University, Johnson City TN 37614

MARK L. GIROUX

Department of Physics and Astronomy, East Tennessee State University, Johnson City TN 37614

CURTIS STRUCK

Department of Physics and Astronomy, Iowa State University, Ames IA 50011

MARK HANCOCK

Department of Physics, University of California Riverside, Riverside CA 92521

SABRINA HURLOCK

Department of Physics and Astronomy, East Tennessee State University, Johnson City TN 37614

Accepted by the Astronomical Journal.

ABSTRACT

We have used the GALEX ultraviolet telescope to study stellar populations and star formation morphology in a well-defined sample of 42 nearby optically-selected pre-merger interacting galaxy pairs. Galaxy interactions were likely far more common in the early Universe than in the present, thus our study provides a nearby well-resolved comparison sample for high redshift studies. We have combined the GALEX NUV and FUV images with broadband optical maps from the Sloan Digitized Sky Survey to investigate the ages and extinctions of the tidal features and the disks. The distributions of the UV/optical colors of the tidal features and the main disks of the galaxies are similar, however, the tidal features are bluer on average in NUV – g when compared with their own parent disks, thus tails and bridges are often more prominent relative to the disks in UV images compared to optical maps. This effect is likely due to enhanced star formation in the tidal features compared to the disks rather than reduced extinction, however, lower metallicities may also play a role. We have identified a few new candidate tidal dwarf galaxies in this sample. Other interesting morphologies such as accretion tails and ‘beads on a string’ are also seen in these images. We also identify a possible ‘Taffy’ galaxy in our sample, which may have been produced by a head-on collision between two galaxies. In only a few cases are strong tidal features seen in HI maps but not in GALEX.

Subject headings: galaxies: starbursts — galaxies: interactions— galaxies: ultraviolet

1. INTRODUCTION

Tidal disturbances have played an important role in reshaping galaxies and triggering star formation over cosmic time (see Struck 1999 for review). H α , far-infrared, and mid-infrared observations show that the mass-normalized star formation rates of pre-merger interacting systems are enhanced by a factor of two on average compared to normal spirals (e.g., Bushouse 1987; Kennicutt et al. 1987; Bushouse, Lamb, & Werner 1988; Barton et al. 2000; Barton Gillespie, Geller, & Kenyon 2003; Smith et al. 2007; Lin et al. 2007). Further, closer

found a larger scatter in the broadband optical colors of Arp Atlas galaxies than isolated galaxies, while Bergvall, Laurikainen, & Aalto (2003) found little color difference between an interacting and a more isolated sample.

Within interacting galaxies, star formation is often enhanced in the nuclear regions compared to the disks (Hummel et al. 1990; Nikolic, Cullen, & Alexander 2004). Luminous star forming regions are sometimes seen in tidal features (Schweizer 1978; Mirabel et al. 1991, 1992; Hibbard & van Gorkom

age—extinction degeneracy in population synthesis modeling (e.g., Smith et al. 2008). Furthermore, since the UV traces somewhat older and lower mass stars (≤ 400 Myrs; O to early-B stars) than $H\alpha$ (≤ 10 Myrs; early- to mid-O stars), it provides a measure of star formation over a longer timescale than $H\alpha$ studies. GALEX imaging of interacting systems have shown that tidal features are sometimes quite bright in the UV (e.g., Neff et al. 2005). In some cases, tidal features previously thought to be purely gaseous have been detected by GALEX (e.g., Hancock et al. 2007). In other systems, GALEX images have been used to identify new tidal features (e.g., Boselli et al. 2005).

To address these issues, we have used the GALEX telescope to image a well-defined sample of more than three dozen strongly interacting galaxies in the ultraviolet. Combined with broadband optical data, these images provide information about the star formation history and dust extinction within the galaxies. For four of the galaxies in this sample (Arp 82, Arp 284, Arp 285, and Arp 305), we have already published the GALEX images as part of detailed studies of the distribution of star formation within the galaxies, and compared with numerical simulations of the interaction (Hancock et al. 2007, 2009; Smith et al. 2008; Peterson et al. 2009). The GALEX images of Arp 24, 85, and 244 were previously analyzed by Cao & Wu (2007), Calzetti et al. (2005), and Hibbard et al. (2005), respectively. In the current paper, we present the full GALEX dataset for the entire sample, compare with optical data, discuss global and tidal properties, and provide a brief discussion of each system. In a followup paper, we compare with a sample of normal galaxies.

The galaxies in our interacting sample were selected to be relatively isolated binary systems, thus they are less complex than many of the interacting systems studied recently by GALEX, for example, the Hickson Group studies by de Mello, Torres-Flores, & Mendes de Oliveira (2008) and Torres-Flores et al. (2009), and the ram-pressure-stripped NGC 5291 system (Boquien et al. 2007). Our galaxies were selected to be relatively simple systems, thus are more amendable to numerical modeling and detailed matching of simulations with multi-wavelength datasets. In the current paper, we provide a summary of the GALEX data for the full sample.

2. THE INTERACTING GALAXY SAMPLE

Our galaxy sample was selected from the Arp Atlas of Peculiar Galaxies (Arp 1966), based on the following criteria: 1) They are relatively isolated binary systems; we eliminated merger remnants, close triples, and multiple systems in which the galaxies have similar optical brightnesses (systems with additional smaller angular

sition, our sample consists of 42 pairs of galaxies. These systems are listed in Table 1. Of these pairs, 13 were already reserved by GALEX guaranteed time projects. We observed the remaining 29 systems (see Section 3). We then combined our new observations with the archival data for the other 13 systems that had already been observed.

This GALEX sample overlaps with the sample that we studied in the infrared using the Spitzer telescope (Smith et al. 2007), however, it is not identical. Spitzer observations were made of some of the galaxies that we were not able to observe with GALEX because of UV-bright stars in the field. In addition, the Spitzer survey omitted galaxies with angular sizes of the individual disks less than $30''$, while these galaxies were included in the GALEX study.

3. OBSERVATIONS

Table 2 provides the dates, exposure times, and tile names for the GALEX observations of our sample, including both our new observations and the archival observations. When possible, we imaged each galaxy for ≥ 1500 seconds in both the far-ultraviolet (FUV) and the near-ultraviolet (NUV) broadband filters of GALEX, which have effective bandpasses of $1350 - 1705\text{\AA}$ and $1750 - 2800\text{\AA}$, respectively. As shown in Table 2, some systems were observed only in NUV or only in FUV, due to a bright star in the field. For the archival study, we only selected galaxies with at least 800 seconds total exposure in either the FUV or NUV. The GALEX field of view is circular with a diameter of 1.2 degrees. The pixel size is $1''.5$, and the spatial resolution is $\sim 5''$. In some cases, the GALEX target position was offset from the position of the galaxy in order to avoid a nearby bright star.

4. OTHER DATA

Of our 42 systems with GALEX data, 29 also have broadband optical images available from the Sloan Digitized Sky Survey (SDSS; Abazajian et al. 2003). These galaxies are identified in Table 2. The SDSS ugriz filters have effective wavelengths of 3560\AA , 4680\AA , 6180\AA , 7500\AA , and 8870\AA , respectively. Of our GALEX sample of 42 pairs, 31 have broadband Spitzer 3.6, 4.5, 5.8, 8.0, and $24\text{ }\mu\text{m}$ images available. Most of these have been published in Smith et al. (2007). Of our 42 systems, 21 have published 21 cm HI maps, while 23 have $H\alpha$ maps available, either from the literature or our own unpublished observations with the Southeastern Association for Research in Astronomy (SARA) telescope. We also have acquired new optical and Spitzer spectra of a few of the star forming regions in some of the tidal features in our sample. These will be discussed in later

pairs with long tails and/or bridges, wide pairs with short tails, close pairs with long tails, and close pairs with short tails. Our sample also includes a possible ‘Taffy’ galaxy, Arp 261, apparently produced by a near head-on collision between two equal-mass gas-rich galaxies, as well as possible previously unidentified ring galaxies in Arp 112, 192, and 282.

Within the tidal features, we see a range of star formation morphologies. In many systems, we see examples of the so-called ‘beads on a string’ morphology, in which regularly-spaced clumps of star formation are seen along spiral arms and tidal features. These clumps are generally spaced about 1 kpc apart, which is the characteristic scale for the gravitational collapse of molecular clouds (Elmegreen & Efremov 1996). Examples of such ‘beads’ are seen in Arp 34, 35, 65, 72, 82, 84, 86, 100, 242, and 285.

In a few systems, we see very luminous star forming regions at the base of a tidal feature. We call these features ‘hinge clumps’ (Hancock et al. 2009). These lie near the intersection of the spiral density wave in the inner disk and the material wave in the tail. These may form when dense material in the inner disk gets pulled out into a tail. This lowers the shear, which may allow more massive clouds to gravitationally collapse. Hinge clumps are seen in Arp 65, 72, 82, 242, 270, and 305.

Our sample also includes some candidate ‘tidal dwarf galaxies’ (TDGs), massive concentrations of young stars near the tips of tidal features. The prototypical TDG in the northern tail of Arp 105 (Duc et al. 1997) is included in our sample, along with the well-studied TDGs in Arp 244 and Arp 245 (Mirabel et al. 1992; Duc et al. 2000). In Arp 242, candidate TDGs are seen in both tails. In Arp 112, in addition to the two main galaxies a third fainter galaxy is seen, which may be either a TDG, a background galaxy, a portion of a collisional ring, or a pre-existing dwarf. In addition, we have identified possible TDGs in Arp 305 (Hancock et al. 2009), Arp 181, and Arp 202. Faint UV clumps are also visible near the end of the long HI tail south of Arp 270, but no optical redshifts are available at present to confirm that these are associated with the tail. These candidate TDGs are discussed in detail in Section 7.

Our sample also contains numerous examples of accretion from one galaxy to another. One of the best-studied examples is the northern tail of Arp 285, which was likely produced from material accreted from the southern galaxy (Toomre & Toomre 1972; Smith et al. 2008). According to our numerical simulations, the material in this tail fell into the gravitational potential of the northern galaxy, overshot that potential, and is now gravitationally collapsing and forming stars (Smith et al. 2008). We call such features ‘accretion tails’, to distin-

Section 7.

Our sample contains only a few tidal features that have high HI column densities ($\sim 4 \times 10^{20} \text{ cm}^{-2}$) but are not detected in our GALEX maps or published optical maps: Arp 84, Arp 269, Arp 270, and Arp 280. A few additional tidal features have somewhat lower HI column densities, between $6 \times 10^{19} \text{ cm}^{-2}$ and 10^{20} cm^{-2} , but no GALEX/SDSS counterparts: Arp 85, 86, and 271. Deeper GALEX and optical images are needed to check whether these are truly starless structures. These features are discussed in more detail in Section 7.

6. UV – OPTICAL COLORS

6.1. Photometry

Magnitudes in the various GALEX and SDSS bands for the main disks and the tidal features are given in Table 3. For the systems with possible TDGs near the tips of tidal features, we determined the colors of the TDG separately from the connecting tail. These are labeled ‘TDG’ in Table 3, although we emphasize that in most cases it is unclear whether these are truly TDGs. These features are discussed in detail in Section 7.

To determine these magnitudes, we used a set of rectangular boxes that covered the observed extent of the targeted area in the GALEX and SDSS images, but avoided very bright stars. These boxes generally coincide with those used in our Spitzer study (Smith et al. 2007), but for some galaxies these were modified, for example, if the observed extent of the tidal features or the disk was larger in the GALEX images. For each system, the sky was measured in a set of rectangular areas without bright stars or galaxies. The uncertainties in Table 3 include both the statistical uncertainty and an uncertainty due to variations from sky region to region, as in Smith et al. (2007). The magnitudes in Table 3 were corrected for Galactic extinction as in Schlegel, Finkbeiner, & Davis (1998), using the Fukugita et al. (2004) extinction law in the SDSS bands and the Cardelli, Clayton, & Mathis (1989) law in the UV. The fluxes were converted to magnitudes on the AB system (Oke 1990) using zero point fluxes of 3631 Jy in each band.

For the three galaxy pairs that span two SDSS fields (Arp 85, 101, and 285), the optical images shown are the mosaicked SDSS images from Hogg et al. (2007). However, the magnitudes quoted in Table 3 for Arp 101 and 285 were measured on the original unmosaicked images. For Arp 270 and 297, we also had to use adjacent SDSS images to do the SDSS photometry of the ends of the tails. For Arp 85, the angular size is so large that sky measurements on the SDSS images is problematic, thus we do not provide SDSS magnitudes.

range of $0.1 - 100 M_{\odot}$. This version of the code includes the Padova asymptotic giant-branch stellar models (Vázquez & Leitherer 2005). We display both solar metallicity and 0.2 solar metallicity models on these plots. We convolved the model spectra with the SDSS and GALEX filter response functions to obtain the model colors shown in Figures 19 – 23.

As in our Arp 285 paper (Smith et al. 2008), to these model colors we added in the $H\alpha$ line, which can contribute significantly to the r band flux for very young ages. We note that this effect is redshift-dependent. For the models plotted in Figures 19 – 23, for the $H\alpha$ line we assumed the velocity of Arp 285, which is typical of the sample as a whole (Table 1). At this redshift, for very young star forming regions ($1 - 5$ Myrs), the r magnitude decreases by $1.1 - 0.25$ magnitudes due to the presence of $H\alpha$ (Smith et al. 2008). However, for our highest redshift objects, the $H\alpha$ line is shifted to the edge of the r band filter where the sensitivity is down by a factor of ~ 2.5 . For these high redshift galaxies, the model r magnitudes plotted in Figures 19 – 23 for very young ages are too bright. The effect of $H\alpha$ is illustrated in Figure 21, the $g - r$ vs. $u - g$ plot, in which we show tracks with and without $H\alpha$. For the rest of the plots, we only display the models which include $H\alpha$. Note that the plotted models do not include the $[O III] \lambda 5007$ or $H\beta$ line, which can contribute substantially to the g filter for low metallicity young galaxies (e.g., Krüger, Fritze-Alvensleben, & Loose 1995; West et al. 2009).

In Figures 24 – 28, we provide histograms of various colors for the main bodies of the galaxies, the tidal features, and the candidate TDGs separately. Selected features are labeled in these figures. For the main bodies of the interacting galaxies, there is a range of colors, reflecting a range in star formation histories, extinction, and progenitor morphological types. For example, the four reddest disks in FUV – NUV are all apparently early-type galaxies: Arp 173 N (classified as S0 in NED¹), Arp 100 S = IC 19 (classified as E in NED), Arp 290 S = IC 195 (classified as SAB0 in NED), and Arp 120 N = NGC 4435 (classified as SB0 in NED). The UV colors of the fifth reddest disk in FUV – NUV, Arp 89 W (= KPG 168 B), may be strongly affected by extinction, since it is an edge-on disk galaxy classified as Sc in NED. For comparison, in the Nearby Galaxies Atlas (Gil de Paz et al. 2007), there is a correlation of FUV – NUV with morphological type, with the early-type galaxies (E/S0) being redder, with FUV – NUV between $1 - 2$, consistent with our reddest systems.

In contrast, many of the bluest disks in our interacting sample have very late morphological types according to NED. For example, in NUV – g the bluest disks are Arp 202 S (Im pec), Arp 24 main (SABm), and Arp 305

Kolmogorov-Smirnov (K-S) tests cannot rule out the possibility that the colors of the disks, the tails/bridges, and the TDGs come from the same parent population. The most significant difference is found for $g - r$, where the tidal features are slightly bluer than the disks, and a K-S test gives a 2.5% probability that the two samples come from the same population. This result is suggestive, but inconclusive. Schombert, Wallin, & Struck-Marcell (1990) also found possibly bluer $B - V$ colors (approximately $g - r$) for the tidal features than the disks, while their $V - i$ colors (approximately $r - i$) for the main bodies and tidal features were similar. We note that the Schombert, Wallin, & Struck-Marcell (1990) sample contains more early-type galaxies than our sample. It also contains a number of merger remnants, which were excluded from our sample. The main bodies of these galaxies are likely redder on average than our sample galaxies due to older stars or more extinction.

Comparison of the colors of the tidal features with the population synthesis models (Figures 19 – 23) show that, in general, the light from both the disks and the tidal features is not dominated by very young stars, and these features are not completely extinction-free. As with the main bodies of these galaxies, there is a range of colors for the tidal features, due to a range in star formation properties and original morphologies. For example, the three tails that are reddest in FUV – NUV are the two broad diffuse tails of Arp 283 and the southern tail in Arp 173, which extends from a red S0 galaxy. No clumps of star formation are visible in these tails. In contrast to these features, the bluest tail in FUV – NUV is Arp 120 WT, with FUV – NUV = -0.03 . This feature was originally discovered by Boselli et al. (2005) using these same GALEX images.

6.3. The Colors of the Tidal Features vs. their Parent Disks

Another useful test is to compare the colors of the individual tidal features with the colors of their own parent disk, rather than with the sample as a whole. In Figure 29, in the various colors we provide histograms of the differences between the colors of the disk and the colors of their matching tidal features. For the bridges, we matched with the most probable progenitor disk of the two galaxies. We matched the northern Arp 285 tail and the southern Arp 105 tail with the southern and northern galaxies in those pairs, respectively, as those are the most likely progenitors (see Section 7).

For most of the histograms in Figure 29, the distributions of color differences peak near zero, and the mean color difference is smaller than the average measurement uncertainty. For NUV – g , however, there is a significant shift of the histogram to the right of zero, with the mean

the candidate tidal dwarf galaxies, which were measured separately. As seen in Figure 25, for Arp 181, 202, and 305, the TDGs are considerably bluer in $\text{NUV} - g$ than their parent tidal features. The inclusion of these regions as part of the tidal feature would increase the difference in color from their associated disk.

Inspection of the population synthesis models plotted in Figure 20 shows that a shift to the blue for $\text{NUV} - g$ without a strong change in $g - r$ is likely an age effect rather than an extinction effect. With the GALEX data, we are able to break the age-extinction degeneracy to a certain extent. Thus we suggest that the stars in the tidal features are younger, on average, than those in their parent galaxies, and star formation, rather than dust extinction, is the primary factor responsible for the bluer $\text{NUV} - g$ colors.

In addition to age, another factor that may be important is metallicity. In general, lowering the metallicity makes the $\text{NUV} - g$ colors bluer (see Figure 20). Of all the colors investigated in this study, $\text{NUV} - g$ is the most strongly affected by metallicity. Since tidal features tend to be drawn from lower metallicity regions in the outer disks, tails and bridges likely have lower abundances than their parent galaxies on average. Thus the observed difference may be due in part to lower metallicities in the tidal features. Only a handful of the tidal features in our sample have available oxygen abundances, which range from $\log(\text{O}/\text{H}) + 12$ of 8.4 to 8.7, or $\sim 1/3 - 1/2$ solar (see Section 7). More direct measurements of abundances in our sample galaxies would be useful to better distinguish between age and metallicity as the cause for this color difference.

6.4. Colors of Subsets of the Sample

As noted in Section 5, our sample is comprised of pre-merger interacting pairs of galaxies with a large variety of morphologies. The sample includes both close pairs and wide pairs, equal mass pairs as well as unequal mass pairs, and pairs with long tails as well as pairs with short or weak tails. To investigate whether any of these subtypes of interacting galaxies stands out from the rest of the sample in their UV/optical colors, we have selected four different subsets from the sample, two selected based on morphology, and two based on pair separation. First, we divided the sample into two groups based on pair separation with the ‘wide pairs’ being the 15 pairs with separations greater than or equal to 30 kpc, and the ‘close pairs’ sample being the 27 galaxies with separations less than 30 kpc (see Table 1). Next, we created a subset including the 10 M51-like galaxies in the sample (see Table 1). Finally, we separated out another subset that includes the 10 pairs with disturbed disks but with weak or no tidal features visible in the optical/UV images. In

of the sample (Smith et al. 2007). In contrast to our results for the SB&T galaxies, earlier studies based on $\text{H}\alpha$ equivalent widths and optical spectroscopy detected a significant difference in star formation rate between close and wide pairs, though with a large amount of scatter (Barton et al. 2000; Lambas et al. 2003; Nikolic, Cullen, & Alexander 2004). Our different conclusions are likely caused in part to selection effects. Our pairs were selected based on the presence of strong tidal distortion. Many of our widely-separated pairs have very long tidal features, which indicates that they probably were closer together at some point in the past, and have already undergone a strong gravitational encounter. In contrast, in the earlier studies, pairs were selected based solely on proximity in space, and thus many of the wider pairs may not have experienced such strong tidal disturbances. Another factor is simply sample size, as our subsets of galaxies are quite small, compared to these earlier studies. Larger sample sizes are needed to further investigate whether particular classes of interacting galaxies are more likely to have enhanced UV/optical colors than other types.

6.5. UV/Optical Colors vs. Spitzer IR Colors

Broadband colors in both the UV/optical range and in the mid-infrared regime are sometimes used as indicators of recent star formation in galaxies, however, each method has advantages and disadvantages. Younger stars have bluer UV/optical colors, however, dust extinction and/or metallicity differences can redden these colors, confusing the issue. The Spitzer 3.6 μm broadband filter is generally assumed to be dominated by the stellar continuum from the older stellar population, while the 24 μm band is dominated by emission from hot dust heated by UV photons from young stars, thus redder [3.6 μm] – [24 μm] color are associated with younger stellar populations on average (e.g., Smith et al. 2007). This is also the case for the [3.6 μm] – [8.0 μm] color, however, in addition to hot dust the Spitzer 8 μm band also includes the prominent interstellar polycyclic aromatic hydrocarbon (PAH) features, which can vary from galaxy to galaxy depending upon the chemistry and the hardness of the UV radiation field. In addition, in extreme starbursts, interstellar contributions can be significant in the 3.6 μm Spitzer band (Smith & Hancock 2009).

To determine how well the colors in these two wavelength regimes correlate, in Figure 31 we compare the Spitzer [3.6] – [24] and [3.6] – [8.0] colors for the disks and tidal features in our sample with their GALEX/SDSS FUV – NUV, NUV – g, and g – r colors. The Spitzer magnitudes were obtained from Smith et al. (2007) when possible. For the galaxies in our current sample that are not in Smith et al. (2007), when Spitzer

gions that match the regions used for the GALEX/SDSS fluxes.

Very weak trends are apparent in some of the panels of Figure 31, in that galaxies that are bluer in $\text{NUV} - g$ and $g - r$ tend to have redder Spitzer $[3.6] - [24]$ and $[3.6] - [8.0]$ colors. However, a very large amount of scatter is present in these plots, and there are galaxies with both red Spitzer colors and red UV/optical colors.

There are several likely reasons for the large scatter in these plots. One factor is system-to-system variations in the geometry of the stars and dust, leading to larger UV/optical extinctions in some systems than others, for the same dust emission. In addition, the dust properties, the metallicities, and the PAHs vary from galaxy to galaxy, along with the strength and hardness of the interstellar radiation field. Furthermore, these fluxes were measured over large regions within the galaxies, entire disks or tidal features, thus they are the sums of the fluxes from multiple star forming regions with different ages and extinctions, combined with the emission from more quiescent regions.

This latter point is illustrated in Figure 32, in which we plot $[3.6] - [8.0]$ vs. $\text{NUV} - g$ and $g - r$ for individual star forming clumps within Arp 285, using the photometry from Smith et al. (2008). The magenta open diamonds are points from the northern tail, the cyan open circles are clumps in the NGC 2856 disk, and the black open squares are clumps in the NGC 2854 disk. These clumps show essentially constant, and very red, $[3.6] - [8.0]$ colors for the clumps, implying very young stellar populations. In contrast, there is a large spread in $\text{NUV} - g$ and $g - r$ for these clumps, indicating a large range of extinction in these clumps. From population synthesis of the UV/optical colors for the individual clumps, we determined extinctions that range from $E(B - V) = 0.1$ to 0.3 for the clumps in the tidal features, to 0.2 to 1.3 for the disk clumps (Smith et al. 2008). For most of these clumps the inferred stellar ages are quite young, $4 - 20$ Myrs, but with large uncertainties.

Comparison of Figure 32 with the two upper right panels in Figure 31 show that individual star forming regions populate a different part of these color-color plots than galaxies as a whole. This is likely due to significant contributions from the underlying older stellar population to the global Spitzer $3.6 \mu\text{m}$ flux densities, as well as to the broadband optical fluxes. This example demonstrates the importance of spatially-resolved measurements in interpreting UV/optical/IR colors in terms of extinction and stellar ages in galaxies.

7. NOTES ON INDIVIDUAL SYSTEMS

Arp 24: Arp 24 (Figure 1) is an M51-like system, but with only a weak bridge. In spite of the very long ex-

tical images. The brightest of the galaxies, NGC 4615, has prominent ‘beads’ of star formation in its inner disk in the GALEX images. It also has an unusual extension to the northwest, which extends out from the disk at an angle. This feature is detected in the $\text{H}\alpha$ map of Gavazzi et al. (2003, 2006), thus it is at the same redshift as Arp 34. The tip of the tail is quite bright in $\text{H}\alpha$ and is faintly visible in the Spitzer $8 \mu\text{m}$ image (Smith et al. 2007). This feature is also quite blue in $\text{NUV} - g$. The similarity of this feature to the Arp 285 accretion tail (Smith et al. 2008) suggests that it may also have been caused by accretion, however, unlike Arp 285, there is no obvious optical bridge between the two galaxies, and no HI map is available at present for Arp 34. NGC 4615 also has a second tail extending to the south towards NGC 4614, which is quite blue in $\text{NUV} - g$.

Arp 35: Arp 35 (Figure 15) is a widely separated M51-like system. The brighter northern galaxy has strong tails with bright knots of star formation, with a hinge clump at the base of the southern tail. The southern galaxy has two short tails. The southern tail of the smaller southern galaxy is the second bluest tidal feature in $\text{FUV} - \text{NUV}$, after the northern tail of Arp 120. Arp 35 was not observed by SDSS or Spitzer, thus little additional information about this tail is available. It is possible that the UV clump in this tail is an ‘accretion knot’, as in Arp 285. Alternatively, it may be a background quasar. Obtaining an optical spectrum of this source would be very valuable in determining its nature.

Arp 65: Arp 65 (Figure 15) is a widely separated equal mass pair of spiral galaxies. The long northern tail of the western galaxy has a prominent hinge clump near the base of the tail, which shows up brightly in the $8 \mu\text{m}$ Spitzer map (Smith et al. 2007). Beads of star formation are also visible further along this tail. In the southern tail of this galaxy, an offset between the old and young stars is seen in the Spitzer images (Smith et al. 2007).

Arp 72: The GALEX images of Arp 72 (Figure 2) show a long ‘beaded’ tail extending to the east of the main galaxy. This tail is also seen in the SDSS and Arp Atlas optical images, but is more pronounced in the GALEX maps and has very blue $\text{NUV} - g$ colors. The main galaxy of Arp 72, NGC 5996, shows a bar-like structure in the SDSS images, connecting to a prominent spiral arm which extends to the north. The bridge that connects NGC 5996 to the low mass companion NGC 5994 is very bright in the UV, with a prominent hinge clump near NGC 5996. The central portion of this bridge has an oxygen abundance of $\log(\text{O}/\text{H}) + 12 \sim 8.7$ (Hancock et al. 2010). In our SARA $\text{H}\alpha$ map, the bridge and the northern spiral arm are quite bright, but the eastern tail was not detected.

Arp 82: We have already published the GALEX images

of a pair of unequal mass spiral galaxies connected by a bridge formed from material pulled out of the smaller northern galaxy NGC 5394. NGC 5394 also has a second tail extending to the north. Along the inner portion of this tail, a series of ‘beads’ is visible in the SDSS image. The most northern knot along this ‘string’ is bright in the GALEX image, as well as in the Spitzer 8 μm map (Smith et al. 2007) and in $\text{H}\alpha$ (Kaufman et al. 1999). It is unclear whether this northern tail is solely a classical tidal tail, or if there is a second ‘accretion component’ interacting with the tidal gas. Perhaps there are two colliding components in this tail which are triggering star formation, as with the Arp 284 bridge (Struck & Smith 2003).

The larger southern galaxy in Arp 84, NGC 5395, also has two tails. The northern tail of the southern galaxy is visible in GALEX as well as in the Kaufman et al. (1999) HI map. This feature is called the ‘arm extension’ by Kaufman et al. (1999). A bright star in the vicinity makes the GALEX and SDSS photometry of this feature uncertain.

The southern tail of NGC 5395 is visible in the Kaufman et al. (1999) HI map of the system as a large gaseous plume extending to the south of the galaxy. This HI feature is not clearly detected in the GALEX maps, in spite of its relatively high HI column density of $N_{\text{HI}} \sim 4 \times 10^{20} \text{ cm}^{-2}$, and relatively narrow HI line width of $\sim 100 \text{ km s}^{-1}$ (Kaufman et al. 1999). In the GALEX map, no diffuse UV emission is seen in this HI plume, although a few UV-bright clumps are present. No redshifts are available at present for these clumps, thus it is uncertain whether they are associated with the galaxy, or are foreground/background objects. The numerical simulation shown in Kaufman et al. (1999) does not produce this plume, which suggests that it may have formed during an earlier encounter.

Arp 85 (M51; ‘The Whirlpool’): GALEX images of Arp 85 (Figure 3) were previously analyzed by Calzetti et al. (2005), in combination with Spitzer infrared and Hubble Space Telescope optical images. Longer exposure GALEX images are now available (see Table 2), but the long gaseous tail visible to the south of Arp 85 (Rots et al. 1990) is still undetected. This is not surprising, as this feature has a relatively low HI column density of $6 \times 10^{19} \text{ cm}^{-2}$, thus may not have a stellar component. Diffuse UV emission is seen to the north of NGC 5195, the smaller galaxy in the pair. In the FUV map, a row of star forming regions is visible in the bridge and into NGC 5195, however, the underlying disk of NGC 5195 is not visible.

Arp 86: The GALEX images of the M51-like pair Arp 86 (Figure 15) show a clumpy arc of UV emission to the south of the main galaxy, connecting to the compan-

HI maps. This is not detected in the GALEX images.

The compact dwarf galaxy 2MASSXJ23470758+2926531 is visible in the GALEX images to the southeast of the Arp 86 system. There is an HI counterpart to this galaxy, showing that it is at the same redshift as Arp 86 (Sengupta, Dwarakanath, & Saikai 2009). The HI maps also show a concentration of gas to the south of the companion. A UV source is visible in the vicinity of this HI cloud in the GALEX images, but whether it is at the same redshift as Arp 86 is unknown.

Arp 87: In the SDSS images of the equal-mass disk galaxy pair Arp 87 (Figure 4), a swirl of blue stars in a polar ring-like structure encircles the edge-on disk of the northern galaxy. These stars likely formed from gas accreted from the southern galaxy along the bridge. Another arc of young stars is visible to the north of the southern galaxy, probably formed from gas that was pulled out into the bridge and is now falling back on the galaxy.

Two additional small disk galaxies are visible in the Arp 87 field, northeast of the northern galaxy and southeast of the southern galaxy. No redshifts are available for these objects, thus it is unknown whether they are associated with Arp 87.

Arp 100: Arp 100 (Figure 15) is a widely separated elliptical/disk galaxy pair. The northern galaxy has two long tails, with four prominent ‘beads’ visible along the brighter northern tail in the GALEX images.

Arp 101: Arp 101 (Figure 5) is another wide elliptical/disk galaxy pair, with a long tail extending to the north of the northern disk galaxy. Between the two galaxies, a very broad diffuse bridge is visible in the SDSS images. This is also faintly visible in the Arp (1966) Atlas picture, but not in the GALEX images.

Arp 105 (‘The Guitar’): Arp 105 contains one of the best-studied examples of a possible TDG, which lies at the end of a long tail extending to the north of a disturbed spiral. This source is named the ‘TDG’ in Table 3. The spiral in turn is connected by a bridge to an elliptical galaxy to the south of the spiral. Further south of the elliptical is a bright knot of star formation (Stockton 1972) which has also been considered a possible TDG (Duc et al. 1997). In HI maps, both the northern TDG candidate and the southern knot of star formation are luminous, containing $7 \times 10^9 M_{\odot}$ and $5 \times 10^8 M_{\odot}$ of HI, respectively (Duc et al. 1997). Kinematic studies suggest that the northern TDG in Arp 105 may be due in part to a projection effect, while the southern star forming region may be a rotating self-gravitating object (Bournaud et al. 2004). The northern TDG candidate has $\log(\text{O}/\text{H}) + 12 = 8.6$, while the southern knot of star formation has $\log(\text{O}/\text{H}) + 12 = 8.4$ (Duc et al. 1994).

Table 3, this feature is simply called the ‘southern tail’.

Another galaxy northeast of the Arp 105 spiral, VV237d, also shows up brightly in the GALEX images. This galaxy has a velocity that differs from that of the Arp 105 spiral by 2700 km s^{-1} , thus is probably a foreground galaxy.

Arp 107 (‘The Smile’): In the SDSS image (Figure 6), the main disk of Arp 107 shows a prominent spiral arm/partial ring-like structure, connected to a short tail. This galaxy is connected to the elliptical-like companion by a bridge. The basic morphology of this system can be produced by a hybrid model, in between a classical ring galaxy simulation of a head-on small impact parameter collision and a prograde planar encounter (Smith et al. 2005a). In the Spitzer $8 \mu\text{m}$ map, the ring is quite bright, especially in the south, as are two luminous knots of star formation in the northwestern sector of the system (Smith et al. 2005a). The ring and the northwestern knots of star formation are also very bright in the GALEX images, while the companion is relatively faint. In contrast, the northern plume of the northern galaxy has a red $\text{NUV} - g$ color (Table 3) and a blue Spitzer $[3.6] - [8.0]$ color (Smith et al. 2007), thus it contains mostly older stars. There is a bright foreground star in front of the Arp 107 main disk, between the ring and the nucleus (Smith et al. 2005a). This is clearly visible in the SDSS color image as a red point source.

Arp 112: In the SDSS image of Arp 112 (Figure 6), three galaxies are visible: a large angular size disturbed spiral NGC 7806, a more compact galaxy to the southwest named NGC 7805, and a fainter arc-like structure to the east, named KUG 2359-311 (called ‘TDG’ in Table 3). In the Arp Atlas picture, KUG 2359-311 appears to be attached to NGC 7806 by a faint tail in the south. There also may be a faint connection between these two galaxies in the north. However, these features are not visible in the SDSS and GALEX images. No redshift is available yet for KUG 2359-311, thus it is uncertain whether it is part of the Arp 112 system or not. KUG 2359-311 is not particularly blue in the UV–optical colors (see Figure 24 – 28). If KUG 2359-311 is at the same redshift as the rest of Arp 112, it may be either a pre-existing dwarf galaxy or a tidal dwarf galaxy. Alternatively, NGC 7806 and KUG 2359-311 may be the remains of a ring galaxy produced by a collision with NGC 7805. Deeper optical and UV images as well as optical spectroscopy are needed to better determine the nature of these galaxies.

In addition to the possible connection to KUG 2359-311, NGC 7806 has a strong tail extending to the north with two UV-bright clumps. Redshifts are also needed for these sources, to determine whether these are associated with the system.

cluded in the current study have already been published by Boselli et al. (2005), who identified a new tidal feature to the northwest of NGC 4438. This feature (called ‘WT’ in Table 3) is the bluest tail in $\text{FUV} - \text{NUV}$ in our sample, with $\text{FUV} - \text{NUV} = -0.03$.

Arp 173: A long tail is visible to the south of the southern galaxy in Arp 173 (Figure 7). This tail has very red UV/optical colors, perhaps in part because its progenitor is an S0 galaxy with little star formation.

Arp 181: Arp 181 (Figure 8) contains two approximately equal mass spiral galaxies, NGC 3212/5. The galaxy to the northwest, NGC 3212, has a long tail extending to the west. A clump is visible near the end of this tail in the Arp (1966) and SDSS optical images, as well as the GALEX images. This clump (called ‘TDG’ in Table 3) has very blue optical/UV colors ($\text{NUV} - g = 1.1$; one of the bluest in our sample), however, no optical spectrum is available and it was not detected in our SARA $\text{H}\alpha$ map, thus it is unclear whether it is at the same redshift as Arp 181.

Further west, beyond the end of the tail at the edge of the Arp Atlas photograph, another galaxy is visible (called the ‘far west’ galaxy in Table 3). This does not have any obvious link to the tail in any of the images. We have an optical spectrum of this galaxy (Hancock et al. 2010), which shows that it is at the same redshift as Arp 181. It is marginally detected in our $\text{H}\alpha$ map, and is visible in the Spitzer maps. In the SDSS image it looks like a spiral galaxy or a disturbed disk with short tidal tails. It is extremely blue in $\text{NUV} - g$ (1.2 magnitudes). Our optical spectrum implies a relatively low oxygen abundance of $\log(\text{O}/\text{H}) + 12 = 7.8$. This may be either a pre-existing dwarf galaxy or a recently detached TDG.

Arp 192: The peculiar system Arp 192 (Figure 8) has a very long distorted tail that curves to the south and then to the east. In the SDSS images, the main body of this system appears to be a very close pair, with a disk galaxy containing a ring galaxy-like loop and a second compact galaxy. In the Arp (1966) Atlas photograph of Arp 192, a straight jet-like feature is seen extending to the northwest out of the second compact nucleus. This feature is not seen in the SDSS or GALEX images, or in the near-infrared images of Bushouse & Stanford (1992), thus the Arp Atlas feature may be an artifact.

Arp 202: Arp 202 (Figure 9) is a very close interaction between an edge-on disk galaxy in the north and a smaller irregularly-shaped galaxy to the south. The southern galaxy has quite blue optical/UV colors, and a long clumpy tail extending to the west. The tip of this tail is very prominent in the GALEX images. We have an optical spectrum of this source that confirms it is at the same redshift as Arp 202 (Hancock et al. 2010), thus it is another possible TDG. This candidate TDG

In the GALEX data (Figure 9), three UV-bright ‘beads’ are visible along the northern tail. Each is associated with a peak in the HI map of Hibbard & van Gorkom (1996). The most northern HI concentration has been classified a possible TDG based on kinematic information (Bournaud et al. 2004). At the tip of the southern tail, there is another UV-bright concentration in the GALEX maps, which also has an HI counterpart. We classify this as a second possible TDG. Near the base of the southern tail is a UV-bright concentration, another possible ‘hinge clump’.

Arp 244 (‘The Antennae’): The interacting pair Arp 244 (Figure 16) has been studied in detail by many authors (e.g., Hibbard et al. 2001; Bastian et al. 2006). A concentration of HI and young stars near the tip of the southern tail of Arp 244 (Schweizer 1978; van der Hulst 1979; Mirabel et al. 1992) has been considered a possible TDG. The GALEX UV images of Arp 244 used in the current study have been previously published by Hibbard et al. (2005), and show that both tails are quite bright in the UV. The southern tail has two parallel ridges of HI and UV emission that meet at the TDG (Hibbard et al. 2001, 2005). This TDG has an oxygen abundance $\log(\text{O}/\text{H}) + 12 \sim 8.4$ (Mirabel et al. 1992).

Arp 245: The possible TDG in the northern tail of Arp 245 was previously studied in the optical, near-IR, HI, and CO by Duc et al. (2000). This source is gas-rich, with an HI mass of $9 \times 10^8 M_\odot$. Young stars are present in this feature, however, the starlight is dominated by light from older stars, with the burst contributing just a small fraction of the observed optical light (Duc et al. 2000). This candidate TDG has possible signs of rotation, however, this is uncertain (Duc et al. 2000). It has an oxygen abundance $\log(\text{O}/\text{H}) + 12 \sim 8.6 - 8.7$ (Duc et al. 2000). In the GALEX maps (Figure 16), the northern tail is bifurcated, as in the Arp 244 tail, with the two strands intersecting near the candidate TDG. A UV-bright foreground star lies in front of the northern tail; this was excluded in the regions used to get the GALEX fluxes.

Arp 253: Arp 253 (Figure 16) is a pair of equal mass edge-on disk galaxies seen end-to-end. No strong tails are visible in this system.

Arp 254: Arp 254 (Figure 16) is a pair of equal mass disk galaxies, with the northern galaxy seen face-on, and the southern edge-on. The southern galaxy has short tidal tails.

Arp 261: Arp 261 (Figure 17) may be an example of a ‘Taffy’ galaxy, produced by a direct head-on collision between two equal-mass gas-rich galaxies. During such collisions, the impact may be sufficient to ionize the gas and strip it from the disks, leaving a large quantity of gas between the two galaxies (Condon et al. 1993). In

pair has a possible ring-like structure, while an apparent bridge is visible to the northeast between the two galaxies. In the NRAO VLA Sky Survey (NVSS), the radio continuum map shows a bright peak between the two galaxies, suggesting a radio continuum bridge between the two galaxies, as in UGC 12914/5 and UGC 813/6. This needs to be confirmed with higher resolution images. Arp 261 is much closer than the other two Taffy galaxies, at only 27 Mpc, and has a lower B luminosity, suggesting that it may consist of two lower mass dwarf galaxies rather than spirals. In Figure 17, a third galaxy, KTS 52, is visible to the northeast of the pair. This has the same redshift as the other two galaxies, thus is part of the same system.

Arp 269: Arp 269 (Figure 10) is an unequal-mass pair of galaxies connected by a bridge. In both the GALEX and SDSS images, an off-center group of blue star forming regions is visible in the smaller galaxy NGC 4485, as well as along the bridge. As noted by Elmegreen et al. (1998), several of these knots of star formation lie in a tail-like structure extending to the southwest of NGC 4485, towards the bridge. These star formation knots in the bridge and NGC 4485 are also seen in archival Spitzer infrared images.

In the GALEX images, a short (2′) tail-like feature is visible extending to the east of NGC 4490, and some diffuse UV emission is seen to the north of NGC 4490. In the Clemens et al. (1998) HI maps, two large plume-like features are seen extending 10′ (~20 kpc) to the north of NGC 4485 and to the south of the larger galaxy NGC 4490. Neither of these plumes are strongly detected in the GALEX or SDSS images, however, smoothed SDSS images show a possible hint of the southern plume. This lack of UV emission is surprising in light of the relatively high HI column density in the inner 5′ (10 kpc) sections of these plumes of $4 \times 10^{20} \text{ cm}^{-2}$.

It was suggested by Clemens et al. (1998) that the HI plumes in Arp 269 were produced by SN-driven outflow from the main galaxy NGC 4490. Furthermore, Clemens et al. (2000) suggest that the smaller galaxy NGC 4485 passed through the gaseous disk of the larger galaxy NGC 4490, and ram pressure from the collision may have caused an offset in the location of the interstellar gas in NGC 4485, and thus the observed offset in star formation. We suggest an alternative possibility, that the HI plumes are simply gas-rich tidal features, and the star formation in NGC 4485 and along the bridge was triggered by gas flowing from the larger galaxy NGC 4490 to NGC 4485 along the bridge. Thus this may be an example of accretion from one galaxy to another, as in Arp 285. Deeper optical and UV imaging is needed to search for a stellar component to the HI plumes, to distinguish between outflow or tidal origin.

the end, faint UV sources are visible in the GALEX and SDSS maps. The source near the end of the tail (labeled ‘TDG’ in Table 3) has moderate optical/UV colors, while the second source is quite blue in FUV – NUV and NUV – g. These may be extended in the SDSS images. Optical spectroscopy is needed to confirm that these sources are associated with the tail.

The HI maps also show a shorter tail extending to the north from the western side of the pair (Clemens et al. 1999). The base of this tail is visible in the UV and optical images, with two UV-bright knots evident in the GALEX images.

Further south of the Arp 270 pair, the dwarf galaxies IC 2604 and IC 2608 are visible on the GALEX images. These are also present in the HI maps of Clemens et al. (1999), and are at the same redshift as Arp 270.

Arp 271: Arp 271 (Figure 17) is a close pair of grand design spirals seen almost face-on. Between the two galaxies a double bridge is seen. In the GALEX maps, the spiral patterns and the two bridge strands are prominent. The western bridge component has a UV-bright knot which also is present in our SARA H α map, as well as the H α maps of Evans et al. (1996). In the Clemens (1998) VLA HI map, the bridge between the galaxies is visible, along with two faint tail-like structures extending 4’ (30 kpc) to the west from each of the main galaxies. These have relatively low HI surface brightnesses of $8 \times 10^{19} \text{ cm}^{-2}$, thus the lack of associated diffuse UV emission in these features in the GALEX maps is not surprising. Two UV-bright clumps are visible at the base of the southern tail. There is also a UV point source in the northern tail, and another UV source in a faint HI clump to the south of the southern tail. Whether these UV sources are at the same redshift as Arp 271 is unknown. In the Clemens (1998) HI map, a dwarf galaxy named APMUKS B1400004.67-054820.9 is seen 8’ (60 kpc) to the west of the pair, beyond the end of the tails. This galaxy is bright in the GALEX maps.

Arp 280: Arp 280 (Figure 11) is an edge-on disk galaxy (SB(r)b: in NED) with a small irregularly-shaped companion (SBm pec in NED). Neither galaxy has strong tails in the optical or UV. The HI map of Clemens (1998) shows a short ($\sim 1' = 4 \text{ kpc}$) tail to the southeast and a longer ($\sim 4' = 16 \text{ kpc}$) tail to the northwest. These tails are not seen in the GALEX or SDSS images, in spite of the $3\text{--}4 \times 10^{20} \text{ cm}^{-2}$ HI column density.

Arp 282: Arp 282 (Figure 11) may be a collisional ring galaxy; alternatively, it may be a spiral gravitationally disturbed by a smaller companion. It consists of two edge-on disk galaxies, orientated such that their major axes lie perpendicular to each other, with the smaller galaxy being near the major axis of the larger galaxy. The larger galaxy has disturbed spiral arms or ring-like

the portion of the disk closest to the companion (called the ‘bridge’ in Table 3) is tidally disturbed, with star forming regions visible in the GALEX, SDSS, Spitzer, and SARA H α maps. In the SDSS images, the western galaxy NGC 2798 has two broad smooth arms/tails (called ‘north tail’ and ‘south tail’ in Table 3) without obvious clumps. These are less prominent in the GALEX data than in the optical. As noted earlier, these have very red FUV – NUV colors.

Arp 284: In the Arp (1966) Atlas picture of Arp 284, the western galaxy NGC 7714 shows a partial ring, two tails to the west, another tail to the northeast, and is connected to its edge-on companion NGC 7715 by a bridge. Strong star formation is visible in the NGC 7714 disk as well as in the bridge (Smith, Struck, & Pogge 1997). In HI maps, the outer western tail seen in the optical images loops back to the bridge, and another long tail is visible to the far west (Smith & Wallin 1992; Smith, Struck, & Pogge 1997). The basic morphology of this system can be reproduced by a prograde, near-head-on collision (Struck & Smith 2003), with the inner western tail being formed via accretion from the bridge, the HI loop being a classical tidal feature, and the far west HI tail being the end of the eastern tail of NGC 7715, wrapped behind the galaxies. In the GALEX FUV map (Figure 17), the HI loop is detected, while the inner ‘accretion tail’ is very bright. The section of the HI loop that contains a possible ‘ultraluminous X-ray’ (ULX) point source (Smith et al. 2005b) is particularly bright in the UV. The knots of star formation in the bridge are also quite prominent in the UV. In the far west HI tail (Smith & Wallin 1992), a hint of extended emission is seen in the smoothed FUV map. A detailed analysis of the GALEX data, in conjunction with Spitzer and Hubble images, has been conducted by Peterson et al. (2009).

Arp 285: The northern galaxy in Arp 285 (Figure 12), NGC 2856, has a peculiar tail-like structure extending to the north perpendicular to the disk. This is very blue in the GALEX/SDSS colors, being the bluest tail in our sample in g – r. According to our numerical simulations of this system, this feature was produced from material accreted along the bridge from the companion (Smith et al. 2008). The southern galaxy in this system, NGC 2854, has a curved tail extending to the south in the GALEX data, matching the HI tail of Chengalur et al. (1994, 1995). The GALEX and SDSS images of this system have been discussed in detail in Smith et al. (2008).

Arp 290: Arp 290 (Figure 13) contains two unequal mass disk galaxies. The larger more northern galaxy has an apparent bar and two peculiar UV-bright arm-like features. As noted above, the smaller southern galaxy IC 195 is classified as SAB0 and is very red in FUV –

Arp 297 resembles M51, with a face-on grand design spiral NGC 5754 and a smaller compact galaxy NGC 5752. However, in the smoothed GALEX and SDSS images a 5' (90 kpc) long faint tail extending to the west is visible (Figure 33). This feature is also visible in deep optical images (Keel & Borne 2003).

Arp 305: A detailed study of the GALEX and SDSS data for the widely separated pair of spirals in Arp 305 has been published in Hancock et al. (2009). In these images (Figure 14), a luminous collection of young stars is seen between the two galaxies. This is located in a large concentration of atomic gas within a gaseous bridge, as seen in HI maps (van Moorsel 1983). The inferred stellar mass of this bridge source is $1-7 \times 10^6 M_{\odot}$ (Hancock et al. 2009), consistent with it being a low mass tidal dwarf galaxy. Significant tidal debris is also seen around the southern galaxy NGC 4017 in the GALEX maps. According to our numerical simulation of this encounter, the bridge TDG will eventually fall into the primary galaxies, and will not become an independent dwarf galaxy.

NGC 4567: NGC 4567 (Figure 14) is a disturbed pair of spirals without strong tidal tails.

8. SUMMARY

In this study, we presented GALEX UV images of 42 interacting galaxy pairs, and compared with available data at other wavelengths. In these images, we identified numerous examples of ‘beads on a string’ and accretion from one galaxy to another, as well as a few new possible tidal dwarf galaxies and ring galaxies. We also note a possible ‘Taffy’ galaxy in our sample. We compared the distributions of UV – optical colors of the tidal features of our sample galaxies with those of the main disks, and found little difference. However, when comparing tidal features with their own parent galaxies on average they appear somewhat bluer in NUV – g. This effect may be due to recent star formation and/or lower metallicities on average.

This dataset provides a valuable atlas of the rest frame UV morphology for a large set of nearby in-

teracting galaxies with a variety of structures. This dataset will be very useful for interpreting the morphology of distant galaxies. Such studies have recently been done for smaller samples of nearby interacting galaxies, which have been artificially redshifted to high redshifts to compare with distant galaxies (e.g., Overzier et al. 2008; Petty et al. 2009). At high redshifts, the merger rate increases and galaxies appear more perturbed (i.e., Abraham et al. 1996; Lotz et al. 2006). At $z \sim 2$ deep optical ground-based surveys trace the rest frame UV with a resolution of $\sim 0.5''$ (~ 4.2 kpc at $z = 2$). The GALEX beam corresponds to scales of 0.6 – 3.6 kpc for our sample, which nicely matches the best resolution obtained for $z \sim 2$ systems.

In a follow-up paper, we will compare the UV/optical colors of our interacting galaxies with those of a ‘control’ sample of normal spirals, to search for evidence of enhancement in the star formation rate relative to less disturbed systems. Additional planned work includes a detailed comparison of the GALEX and optical images with available HI, H α , and Spitzer maps, to investigate star formation efficiencies and thresholds in the tidal features. We also plan detailed analyses of the spatial distribution of star formation within selected galaxies in the sample. We have acquired ground-based optical spectra and Spitzer infrared spectra of a few of the star forming regions in our sample, which will be presented in future papers (Hancock et al. 2010; Higdon et al. 2010).

We thank the GALEX team for making this research possible. This research was supported by GALEX grant GALEXGI04-0000-0026, NASA LTSA grant NAG5-13079, and Spitzer grants RSA 1353814 and RSA 1379558. This research has made use of the NASA/IPAC Extragalactic Database (NED) and the NASA/IPAC Infrared Science Archive, which are operated by the Jet Propulsion Laboratory, California Institute of Technology, under contract with the National Aeronautics and Space Administration. We also utilized the GOLDMINE database (<http://goldmine.mib.infn.it>).

REFERENCES

- Abazajian, K., et al. 2003, *AJ*, 126, 2081
 Abraham, R. G., van den Bergh, S., Glazebrook, K., Ellis, R. S., Santiago, B. X., Surma, P., & Griffiths, R. E. 1996, *ApJS*, 107, 1
 Arp, H. 1966, *Atlas of Peculiar Galaxies* (Pasadena: Caltech)
 Barton, E. J., Geller, M. J., & Kenyon, S. J. 2000, *ApJ*, 530, 660
 Barton Gillespie, E., Geller, M. J., & Kenyon, S. J. 2003, *ApJ*, 582, 668
 Bastian, N., Emsellem, E., Kissler-Patig, M., & Maraston, C. 2006, *A&A*, 445, 471
 Bergvall, N., Laurikainen, E. & Aalto, S. 2003, *A&A* 405, 31
 Boquien, M., Duc, P.-A., Braine, E., Lisenfeld, U., & Cardelli, J. A., Clayton, G. C., & Mathis, J. S. 1989, *ApJ*, 345, 245
 Chengalur, J. N., Salpeter, E. E., & Terzian, Y. 1994, *AJ*, 107, 1984
 Chengalur, J. N., Salpeter, E. E., & Terzian, Y. 1995, *AJ*, 110, 167
 Clemens, M. S., Alexander, P., & Green, D. A. 1998, *MNRAS*, 297, 1015
 Clemens, M. S. 1998, Ph.D. Thesis, Cambridge University
 Clemens, M. S., Alexander, P., & Green, D. A. 2000, *MNRAS*, 312, 236
 Clemens, M. S., Baxter, K. M., Alexander, P., & Green, D. A.

- Elmegreen, D. M., Chromey, F. R., Knowles, B. D., & Wittenmyer, R. A. 1998, *AJ*, 115, 1433
- Elmegreen, B. G. & Efremov, Y. N. 1996, *ApJ*, 466, 802
- Evans, I. N., Koratkar, A. P., Storch-Bergmann, T., Kirkpatrick, H., Heckman, T. M., & Wilson, A. S. 1996, *ApJS*, 105, 93
- Fukugita, M., Yasuda, N., Brinkmann, J., Gunn, J. E., Ivezić, Z., Knapp, G. R., Lupton, R., & Schneider, D. P. 2004, *AJ*, 127, 3155
- Gavazzi, G., Boselli, A., Cortese, L., Arosio, I., Gallazzi, A., Pedotti, P., & Carrasco, L. 2006, *A&A*, 446, 839
- Gavazzi, G., Boselli, A., Donati, A., Franzetti, P., & Scodreggio, M. 2003, *A&A*, 400, 451
- Gil de Paz, A., et al. 2007, *ApJS*, 173, 185
- Hancock, M., Smith, B. J., Struck, C., Giroux, M. L., Appleton, P. N., Charmandaris, V., & Reach, W. T. 2007, *AJ*, 133, 791
- Hancock, M., et al. 2010, in preparation
- Hancock, M., Smith, B. J., Struck, C., Giroux, M. L., & Hurlock, S. 2009, *AJ*, 137, 4643
- Hibbard, J. E., et al. 2005, *ApJ*, 619, L87
- Hibbard, J. E., van der Hulst, J. M., Barnes, J. E., & Rich, R. M. 2001, *AJ*, 122, 2969
- Hibbard, J. E. & van Gorkom, J. H. 1996, *AJ*, 111, 655
- Higdon, S. J. U., et al. 2010, in preparation
- Hogg, D. W., Blanton, M. R., and the SDSS Collaboration 2007, private communication.
- Hummel, E., van der Hulst, J. M., Kennicutt, R. C. & Keel, W. C. 1990, *A&A*, 236, 333
- Kaufman, M., Brinks, E., Elmegreen, D. M., Thomasson, M., Elmegreen, B. G., Struck, C., & Klaric, M. 1997, *AJ*, 114, 2323
- Kaufman, M., Brinks, E., Elmegreen, B. G., Elmegreen, D. M., Klarić, M., Struck, C., Thomasson, M., & Vogel, S. 1999, *AJ*, 118, 1577
- Keel, W. C. & Borne, K. D. 2003, *AJ*, 126, 1257
- Keel, W. C., Kennicutt, R. C., Jr., Hummel, E., & van der Hulst, J. M. 1985, *AJ*, 90, 708
- Kenney, J. D. P., Rubin, V. C., Planesas, P., & Young, J. S. 1995, *ApJ*, 438, 135
- Kenney, J. D. P., Tal, T., Crowl, H. H., Feldmeier, J., & Jacoby, G. H. 2008, *ApJ*, 687, L69
- Kennicutt, R. C., Jr., Keel, W. C., van der Hulst, J. M., Hummel, E., & Roettiger, K. A. 1987, *AJ*, 93, 1011
- Kroupa, P. 2002, *Science*, 295, 85
- Krüger, H., Fritz-v. Alvensleben, U., & Loose, H.-H. 1995, *A&A*, 303, 41
- Lambas, D. G., Tissera, P. B., Alonso, M. S., & Coldwell, G. 2003, *MNRAS*, 346, 1189
- Larson, R. B. & Tinsley, B. M. 1978, *ApJ*, 219, 46
- Leitherer, C., et al. 1999, *ApJS*, 123, 3
- Lin, L., et al. 2007, *ApJ*, 660, 51
- Lotz, J. M., Madau, P., Giavalisco, M., Primack, J., & Ferguson, H. C. 2006, *ApJ*, 636, 592
- Mirabel, I. F., et al. 1991, *A&A*, 243, 367
- Mirabel, I. F., et al. 1992, *A&A*, 256, L19
- Neff, S. G., et al. 2005, *ApJ*, 619, L91
- Nikolic, B., Cullen, H., & Alexander, P. 2004, *MNRAS*, 355, 874
- Oke, J. B. 1990, *AJ*, 99, 1621
- Overzier, R. A., et al. 2008, *ApJ*, 677, 37
- Peterson, B. W., Struck, C., Smith, B. J., & Hancock, M. 2009, *MNRAS*, in press
- Petty, S. M., de Mello, D. F., Gallagher, J. S., Gardner, J. P., Lotz, J. M., Matt Mountain, C., & Smith, L. J. 2009, *AJ*, 138, 362
- Rots, A. H., Bosma, A., van der Hulst, J. M., Althanssoula, E., & Crane, P. C. 1990, *AJ*, 100, 387
- Schlegel, D. J., Finkbeiner, D. P., & Davis, M. 1998, *ApJ*, 500, 525
- Schombert, J. M., Wallin, J. F., & Struck-Marcell, C. 1990, *AJ*, 99, 497
- Schweizer, F. 1978, in *Structure and Properties of Nearby Galaxies*, ed. E. M. Berkhuijsen & R. Wielebinski (Dordrecht: Reidel), 279
- Sengupta, C., Dwarakanath, K. S., & Saikai, D. J. 2009, *MNRAS*, 397, 548
- Smith, B. J. & Hancock, M. 2009, *AJ*, 138, 130
- Smith, B. J. & Wallin, J. F. 1992, *ApJ*, 393, 544
- Smith, B. J., Struck, C., Hancock, M., Appleton, P. N., Charmandaris, V., & Reach, W. T. 2007, *AJ*, 133, 791
- Smith, B. J., et al. 2008, *AJ*, 135, 2406
- Smith, B. J., Struck, C., Appleton, P. N., Charmandaris, V., Reach, W., & Eitter, J. J. 2005a, *AJ*, 130, 2117
- Smith, B. J., Struck, C., & Nowak, M. A. 2005b, *AJ*, 129, 1350
- Smith, B. J., Struck, C., & Pogge, R. W. 1997, *ApJ*, 483, 754
- Stockton, A. 1972, *ApJ*, 173, 247
- Struck, C. 1999, *Phys. Rep.*, 321, 1
- Struck, C. & Smith, B. J. 2003, *ApJ*, 589, 157
- Toomre, A., & Toomre, J. 1972, *ApJ*, 178, 623.
- Torres-Flores, S., Mendes de Oliveira, C., de Mello, D. F., Amram, P., Plana, H., Epinat, B., & Iglesias-Paramo, J. 2009, *A&A*, in press
- van der Hulst, J. M. 1979, *A&A*, 71, 131
- van Moorsel, G. A. 1983, *A&AS*, 54, 19
- Vázquez, G. A. & Leitherer, C. 2005, *ApJ*, 621, 695
- West, A. W., Garcia-Appadoo, D. A., Dalcanton, J. J., Disney, M. J., Rockosi, C. M., & Ivezić, Z. 2009, *AJ*, 138, 796

FIG. 1.— A comparison of the GALEX images (left) and the SDSS images (right). North is up and east to the left in these figures, as well as in all the subsequent UV and optical images. When both FUV and NUV data are available, the displayed GALEX images are color-coded such that blue is the FUV data, while yellow is the NUV. For the SDSS pictures, the images are approximately true-color. In the Arp 24 SDSS image, the small galaxy in the upper left is a background galaxy.

FIG. 2.— A comparison of the GALEX images (left) and the SDSS images (right), as in Figure 1.

FIG. 3.— A comparison of the GALEX images (left) and the SDSS images (right), as in Figure 1. The SDSS image of Arp 85 (M51) is a mosaic from Hogg et al. (2007).

FIG. 4.— A comparison of the GALEX images (left) and the SDSS images (right), as in Figure 1. In the Arp 87 image, no redshift is available for the third galaxy to the upper left.

FIG. 5.— A comparison of the GALEX images (left) and the SDSS images (right), as in Figure 1. The SDSS image of Arp 101 is a mosaic from Hogg et al. (2007). In the GALEX image of Arp 101, the brightest UV source near the top of the Figure is not part of Arp 101.

FIG. 6.— A comparison of the GALEX images (left) and the SDSS images (right), as in Figure 1.

FIG. 7.— A comparison of the GALEX images (left) and the SDSS images (right), as in Figure 1.

FIG. 8.— A comparison of the GALEX images (left) and the SDSS images (right), as in Figure 1.

FIG. 9.— A comparison of the GALEX images (left) and the SDSS images (right), as in Figure 1.

FIG. 10.— A comparison of the GALEX images (left) and the SDSS images (right), as in Figure 1. The SDSS image of Arp 270 is a mosaic from Hogg et al. (2007).

FIG. 11.— A comparison of the GALEX images (left) and the SDSS images (right), as in Figure 1. A bright star lies to the northeast of Arp 282, beyond the displayed field of view.

FIG. 12.— A comparison of the GALEX images (left) and the SDSS images (right), as in Figure 1. The SDSS image of Arp 285 is a mosaic from Hogg et al. (2007).

FIG. 13.— A comparison of the GALEX images (left) and the SDSS images (right), as in Figure 1. For the Arp 297 images, to the west of the southern pair beyond the extent of this view, a long tail is visible in the smoothed SDSS and GALEX images.

FIG. 14.— A comparison of the GALEX images (left) and the SDSS images (right), as in Figure 1.

FIG. 15.— The GALEX images for the galaxies without available SDSS data. These images are color-coded such that blue is the FUV data, while yellow is the NUV. In the Arp 65 image, the small angular size galaxy to the northeast is a background galaxy.

FIG. 16.— The GALEX images for the galaxies without available SDSS data. These images are color-coded such that blue is the FUV data, while yellow is the NUV.

FIG. 17.— GALEX pictures of sample galaxies without SDSS observations.

FIG. 18.— GALEX pictures of sample galaxies without SDSS observations.

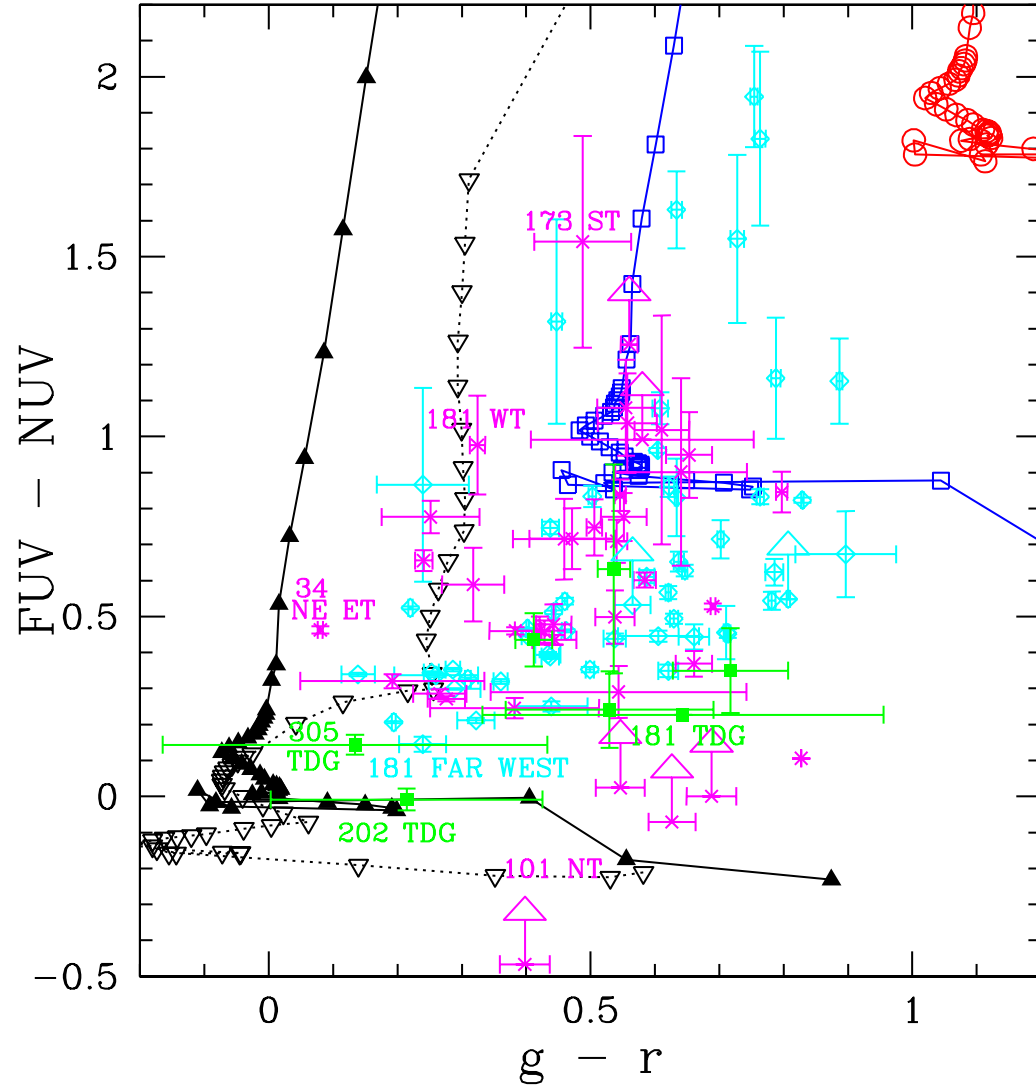


FIG. 19.— The GALEX $FUV - NUV$ vs. $g - r$ colors for the main disks of the interacting galaxy sample (cyan open diamonds) and the tidal features of these galaxies (magenta crosses). The green filled squares are the values for the candidate TDGs, which have been measured separately from their parent tidal features. Some of these features are labeled, in the same color as the corresponding data point. The solar metallicity models have an extinction of $E(B - V) = 0$ (black filled triangles), $E(B - V) = 0.5$ (blue open squares), and $E(B - V) = 1$ (open red circles). The upside down black open triangles are zero extinction 0.2 solar metallicity models. All models include $H\alpha$. The ages are increasing from the bottom starting at 1 Myrs, by step sizes of 1 Myrs to 20 Myrs, then by 5 Myr steps to 50 Myrs, then 10 Myr steps to 100 Myrs, 100 Myr steps to 1 Gyr, and 500 Myr steps to 10 Gyrs.

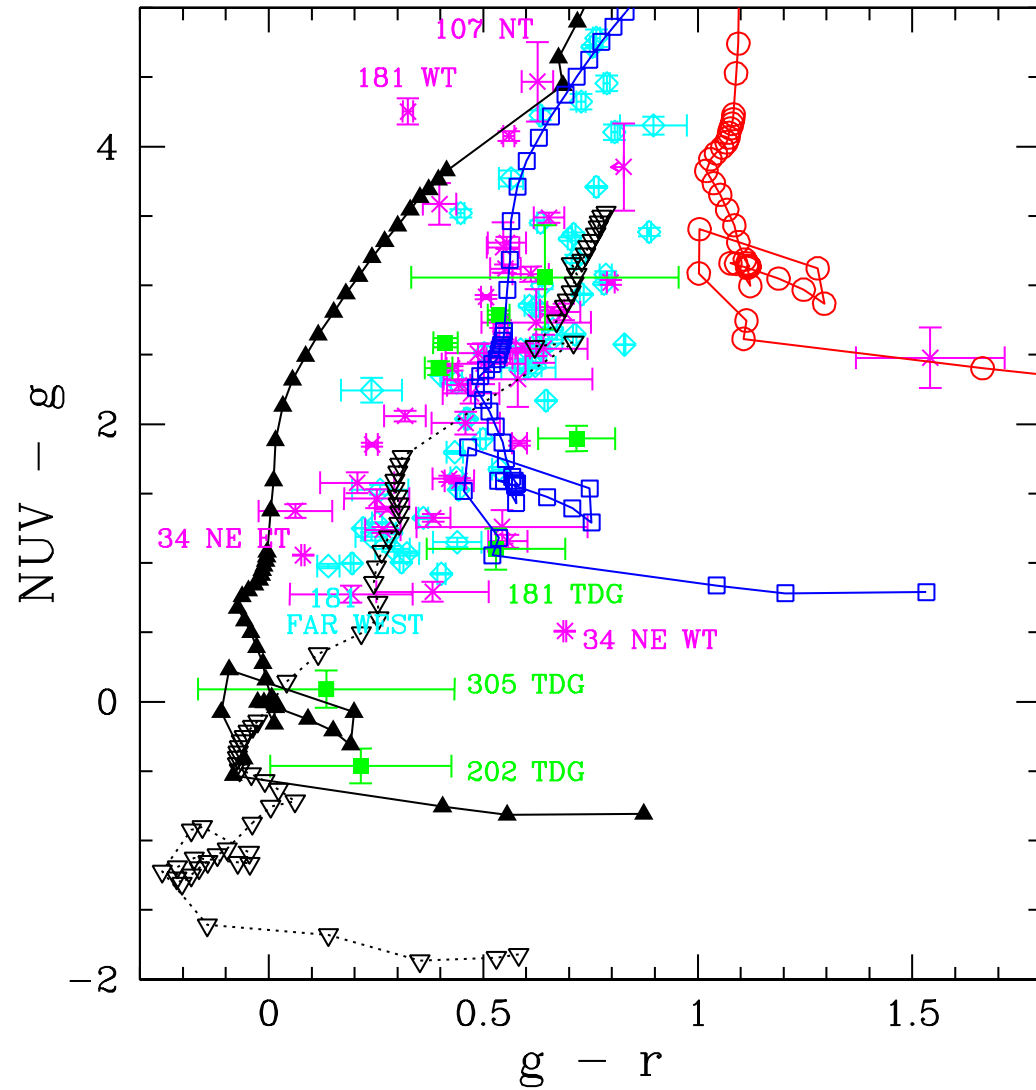


FIG. 20.— The GALEX/SDSS $\text{NUV} - g$ vs. $g - r$ colors for the main disks of the interacting galaxy sample (cyan open diamonds) and the tidal features of these galaxies (magenta crosses). The green filled squares are the values for the candidate TDGs, which have been measured separately from their parent tidal features. The solar metallicity models have an extinction of $E(B - V) = 0$ (black filled triangles), $E(B - V) = 0.5$ (blue open squares), and $E(B - V) = 1$ (open red circles). The upside down black open triangles are 0.2 zero extinction solar metallicity models. All models include $\text{H}\alpha$. The ages are increasing from the bottom starting at 1 Myrs, by step sizes of 1 Myrs to 20 Myrs, then by 5 Myr steps to 50 Myrs, then 10 Myr steps to 100 Myrs, 100 Myr steps to 1 Gyr, and 500 Myr steps to 10 Gyr.

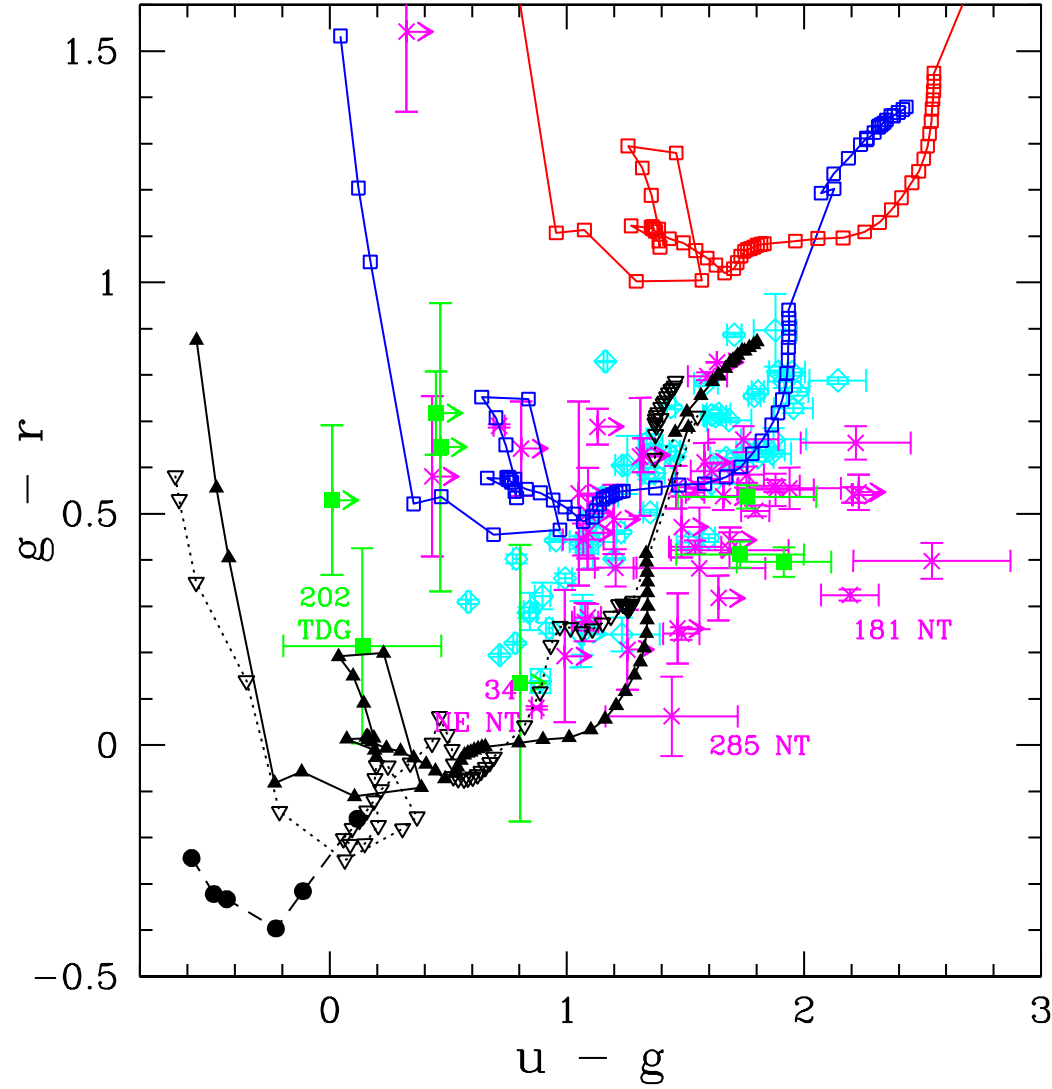


FIG. 21.— The SDSS $g - r$ vs. $u - g$ colors for the main disks of the interacting galaxy sample (cyan open diamonds) and the tidal features of these galaxies (magenta crosses). The green filled squares are the values for the candidate TDGs, which have been measured separately from their parent tidal features. The models have an extinction of $E(B - V) = 0$ (black filled triangles), $E(B - V) = 0.5$ (blue open squares), and $E(B - V) = 1$ (open red circles). The upside down black open triangles are 0.2 zero extinction solar metallicity models. All models include $H\alpha$, except for the filled black circles, which are zero extinction solar metallicity models without $H\alpha$. The ages are increasing from the bottom, by step sizes of 1 Myrs to 20 Myrs, then by 5 Myr steps to 50 Myrs, then 10 Myr steps to 100 Myrs, 100 Myr steps to 1 Gyr, and 500 Myr steps to 10 Gyrs.

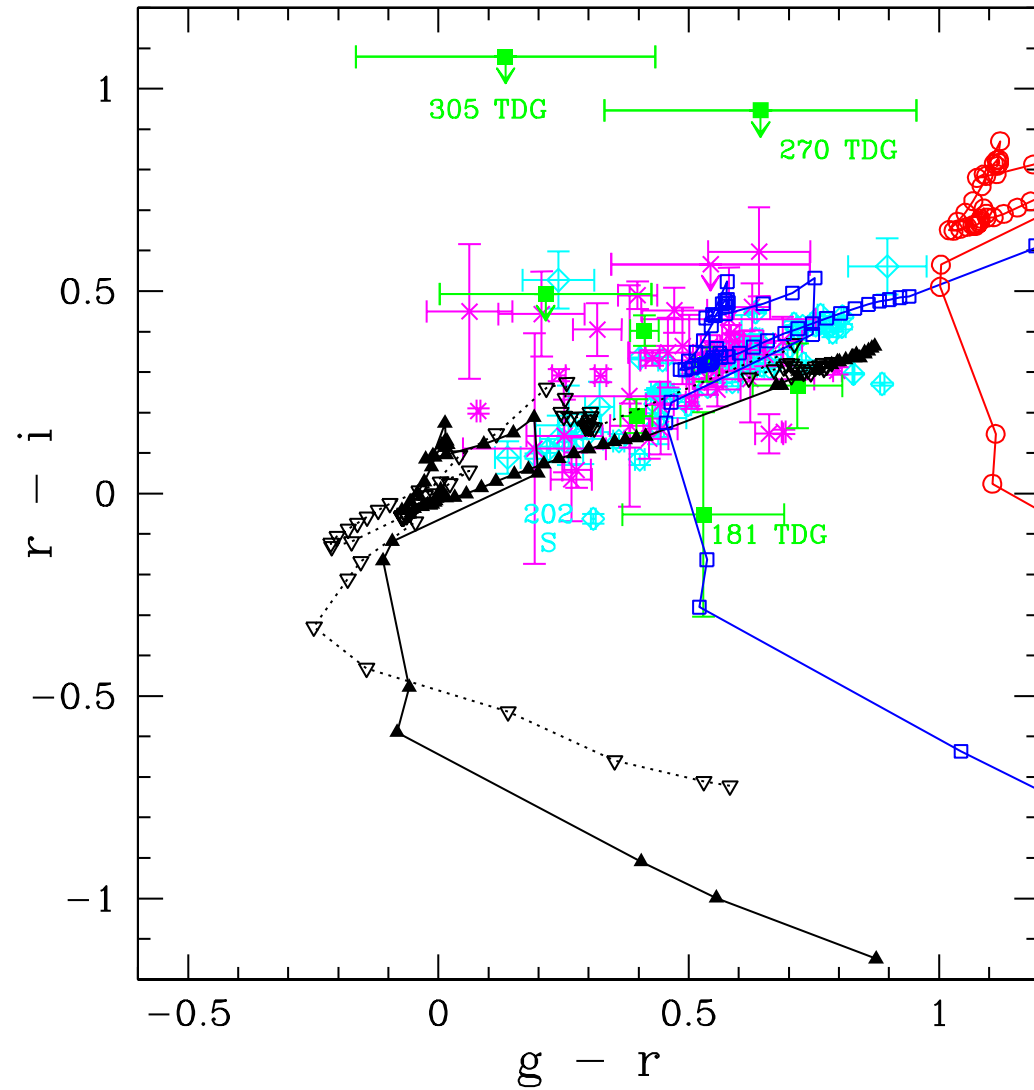


FIG. 22.— The SDSS $r - i$ vs. $g - r$ colors for the main disks of the interacting galaxy sample (cyan open diamonds) and the tidal features of these galaxies (magenta crosses). The green filled squares are the values for the candidate TDGs, which have been measured separately from their parent tidal features. The models have an extinction of $E(B - V) = 0$ (black filled triangles), $E(B - V) = 0.5$ (blue open squares), and $E(B - V) = 1$ (open red circles). The upside down black open triangles are 0.2 zero extinction solar metallicity models. All models include $H\alpha$. The ages are increasing from the bottom, by step sizes of 1 Myrs to 20 Myrs, then by 5 Myr steps to 50 Myrs, then 10 Myr steps to 100 Myrs, 100 Myr steps to 1 Gyr, and 500 Myr steps to 10 Gyrs.

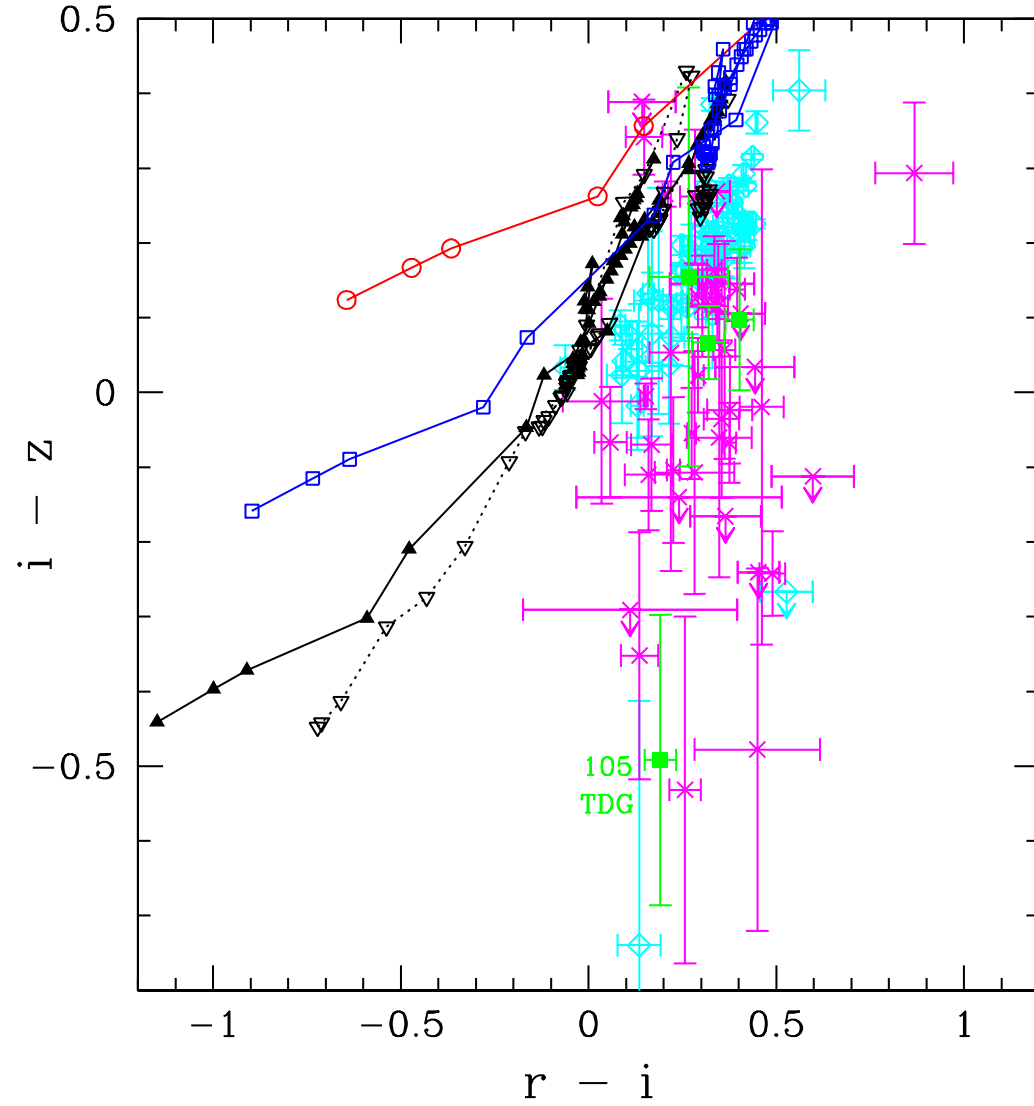


FIG. 23.— The SDSS $i - z$ vs. $r - i$ colors for the main disks of the interacting galaxy sample (cyan open diamonds) and the tidal features of these galaxies (magenta crosses). The green filled squares are the values for the candidate TDGs, which have been measured separately from their parent tidal features. The models have an extinction of $E(B - V) = 0$ (black filled triangles), $E(B - V) = 0.5$ (blue open squares), and $E(B - V) = 1$ (open red circles). The upside down black open triangles are 0.2 zero extinction solar metallicity models. All models include $H\alpha$. The ages are increasing from the bottom starting at 1 Myrs, by step sizes of 1 Myrs to 20 Myrs, then by 5 Myr steps to 50 Myrs, then 10 Myr steps to 100 Myrs, 100 Myr steps to 1 Gyr, and 500 Myr steps to 10 Gyrs.

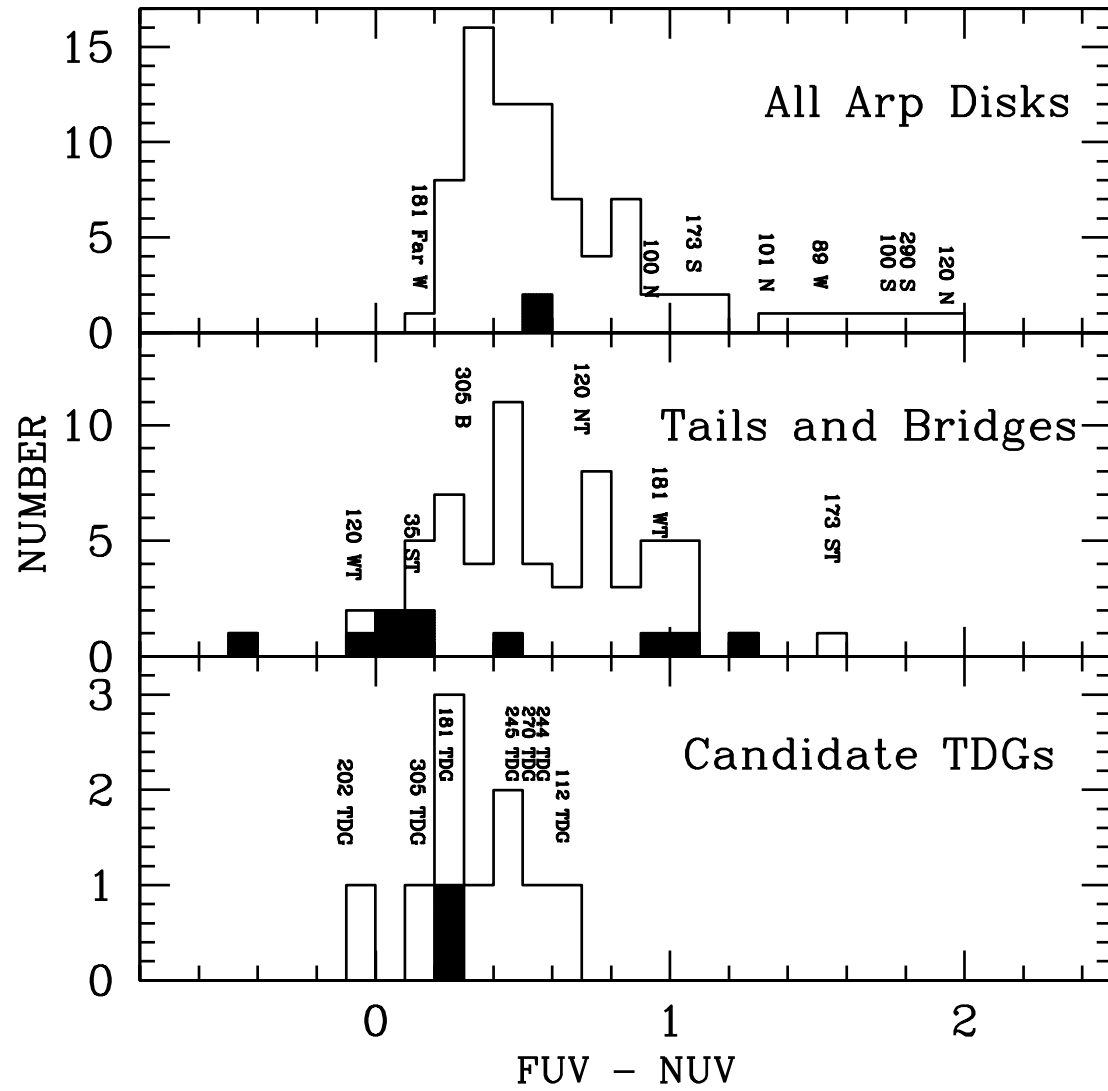


FIG. 24.— Histogram of the $FUV - NUV$ colors of the Arp disks, the Arp tails and bridges, and the TDGs. The filled regions are lower limits.

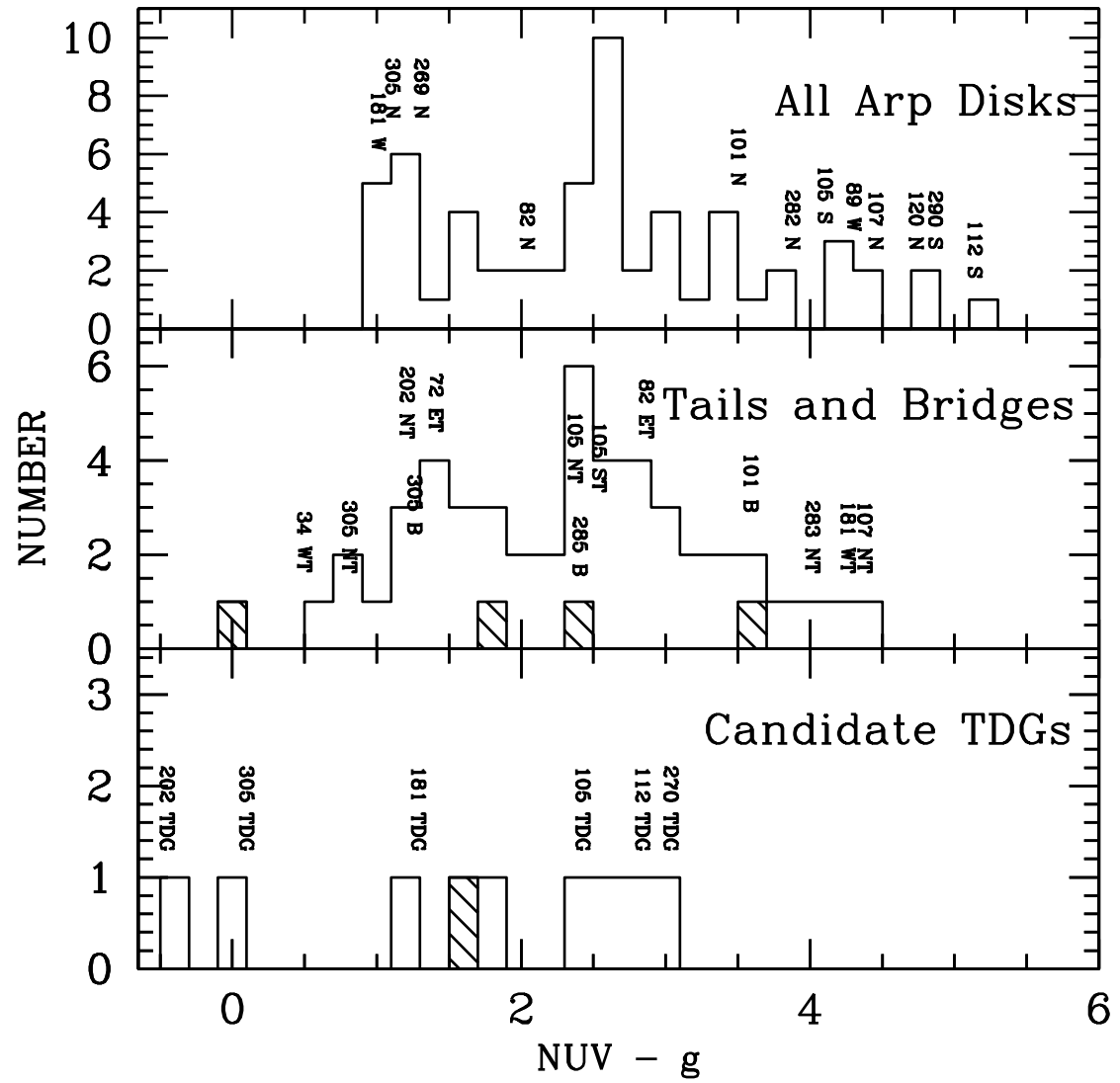


FIG. 25.— Histogram of the $NUV - g$ colors of the Arp disks, the Arp tails and bridges, and the TDGs. The hatched areas are upper limits.

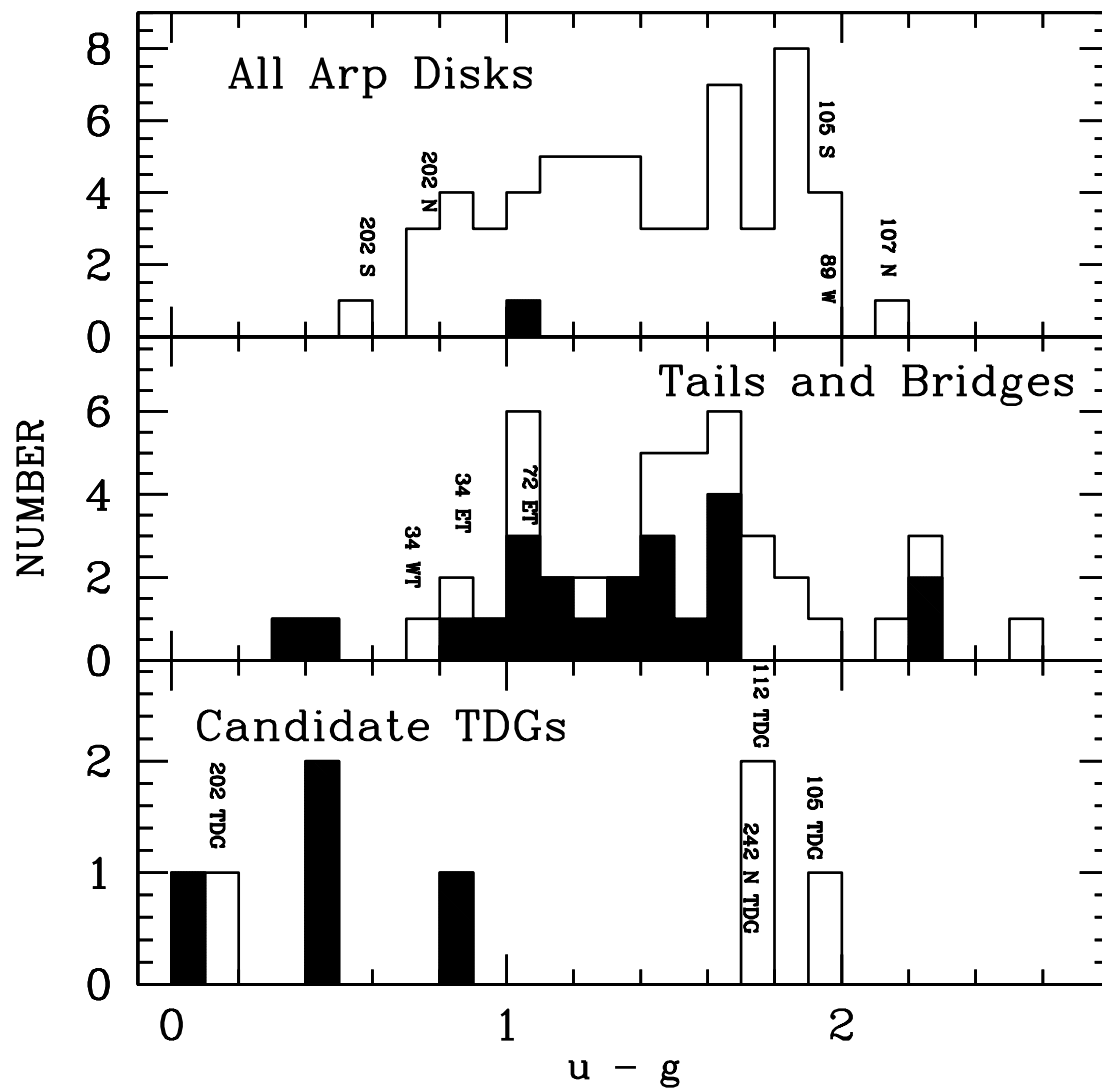


FIG. 26.— Histogram of the $u - g$ colors of the Arp disks, the Arp tails and bridges, and the TDGs. The filled regions are lower limits.

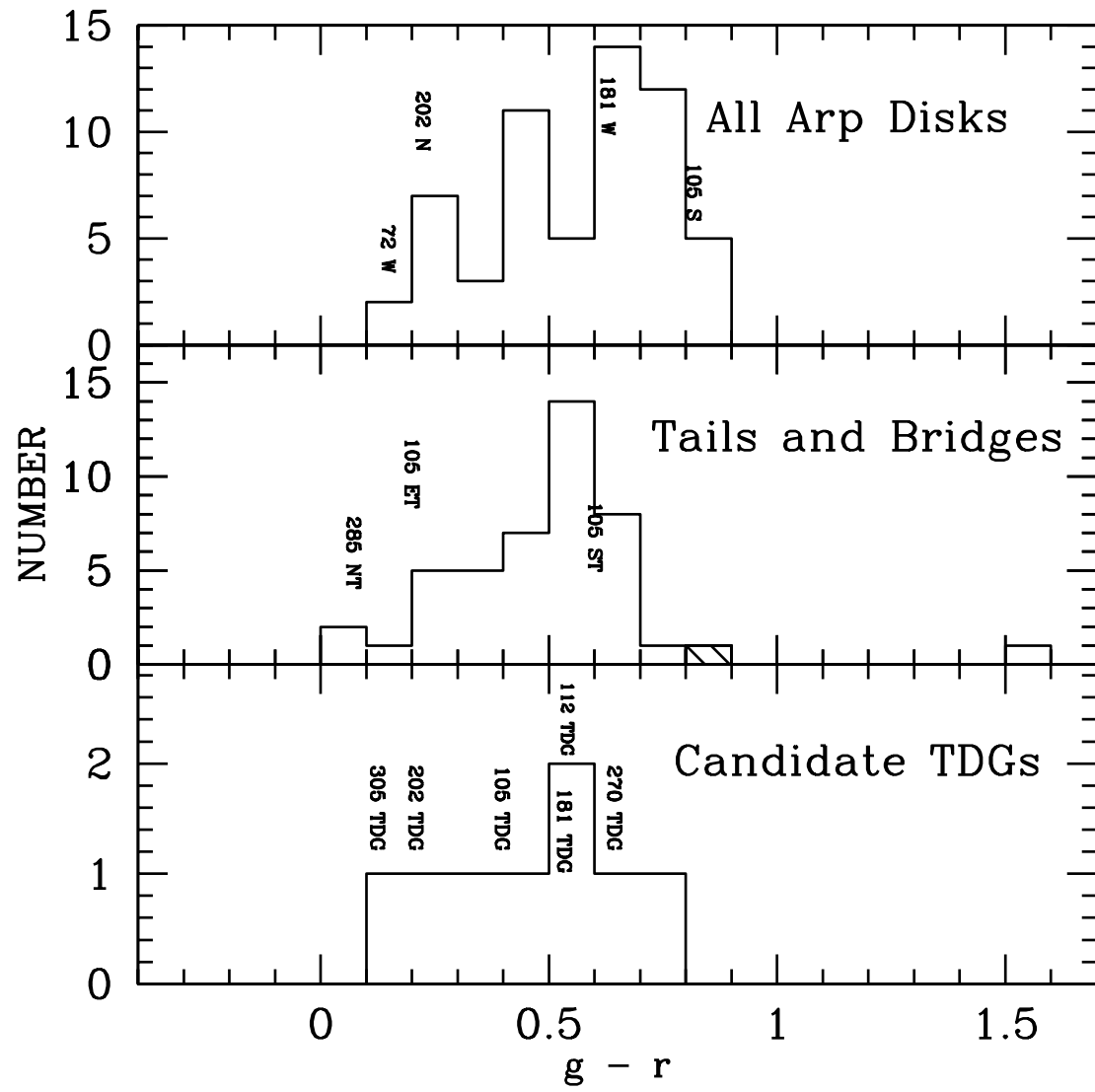


FIG. 27.— Histogram of the $g - r$ colors of the Arp disks, the Arp tails and bridges, and the TDGs. The hatched regions are upper limits.

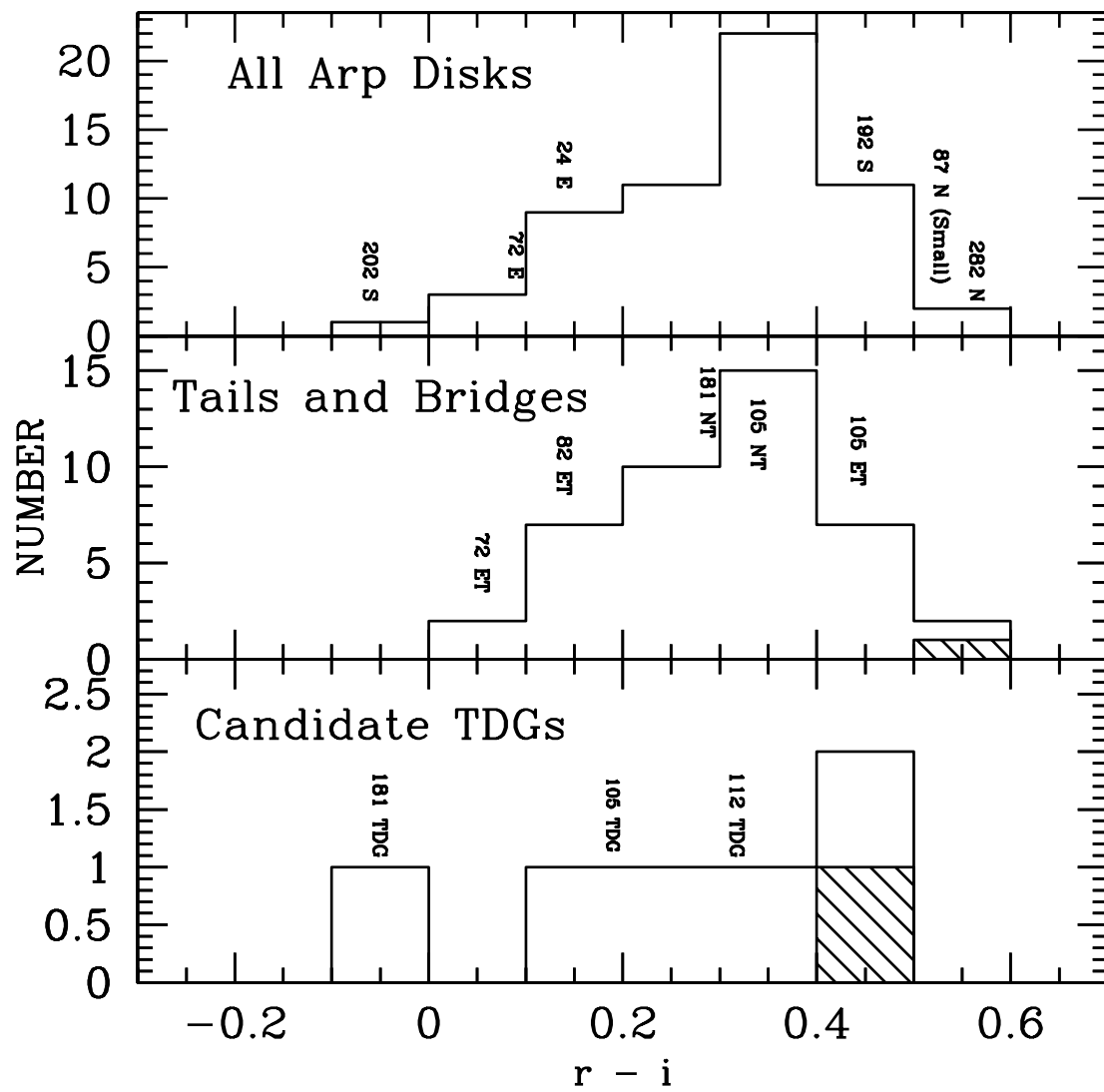


FIG. 28.— Histogram of the $r - i$ colors of the Arp disks, the Arp tails and bridges, and the TDGs. The hatched areas are upper limits.

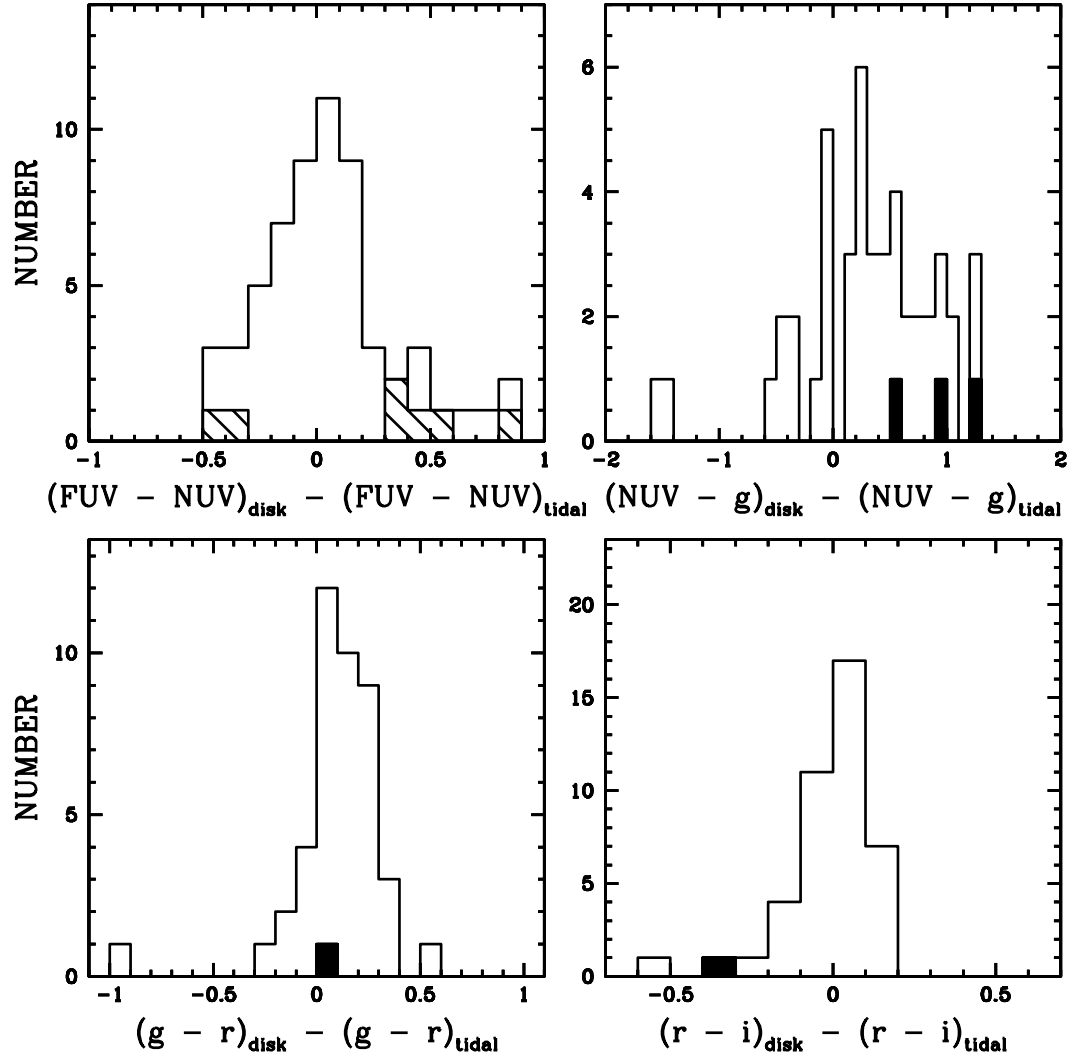


FIG. 29.— Histograms of the difference between the colors of the tidal features and their parent disks. Lower limits are plotted as solid regions, while upper limits are plotted as hatched regions.

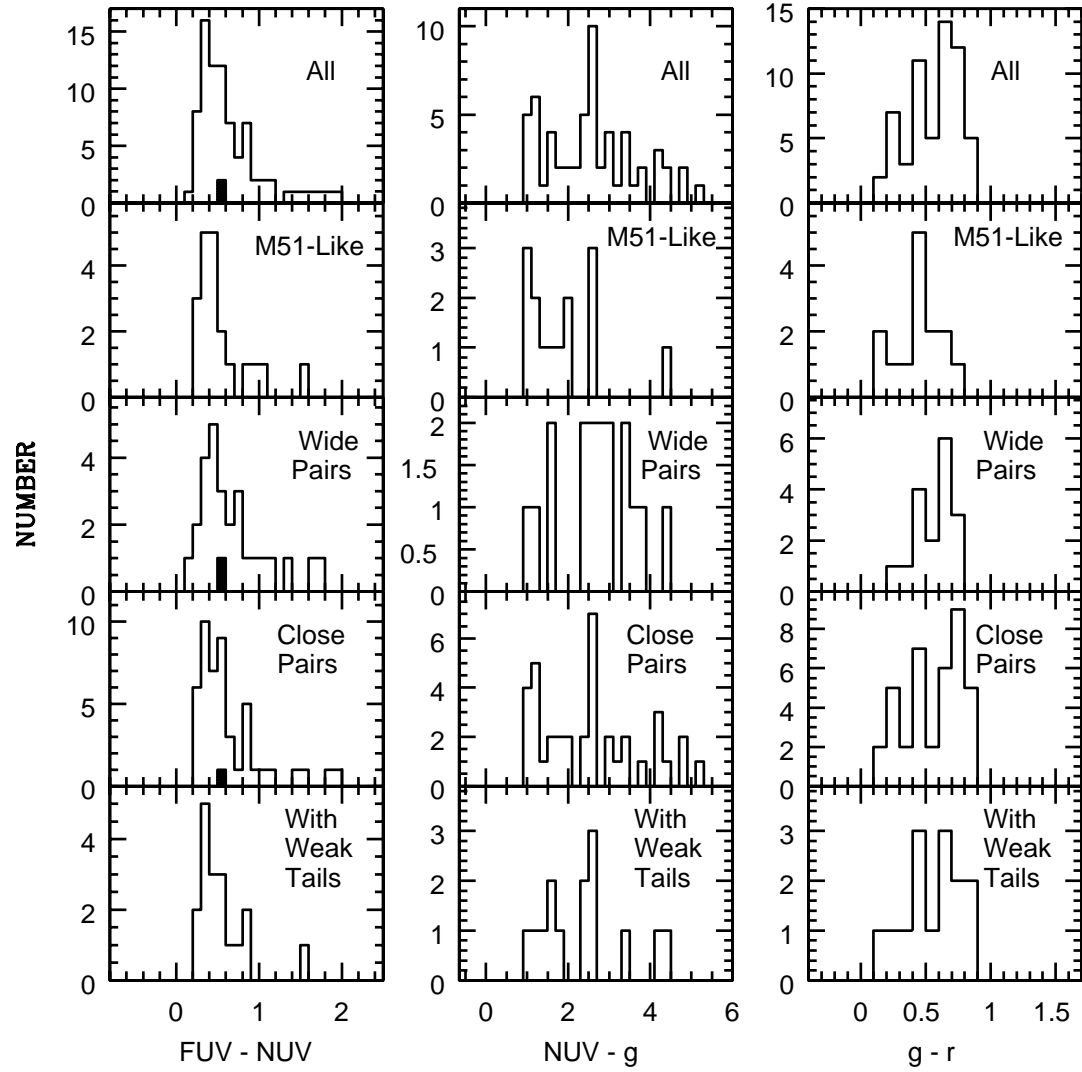


FIG. 30.— Histograms of the $FUV - NUV$, $NUV - g$, and $g - r$ colors of the disks of various subsets of the sample galaxies. The wide pairs are galaxies separated by ≥ 30 kpc. The filled regions are lower limits.

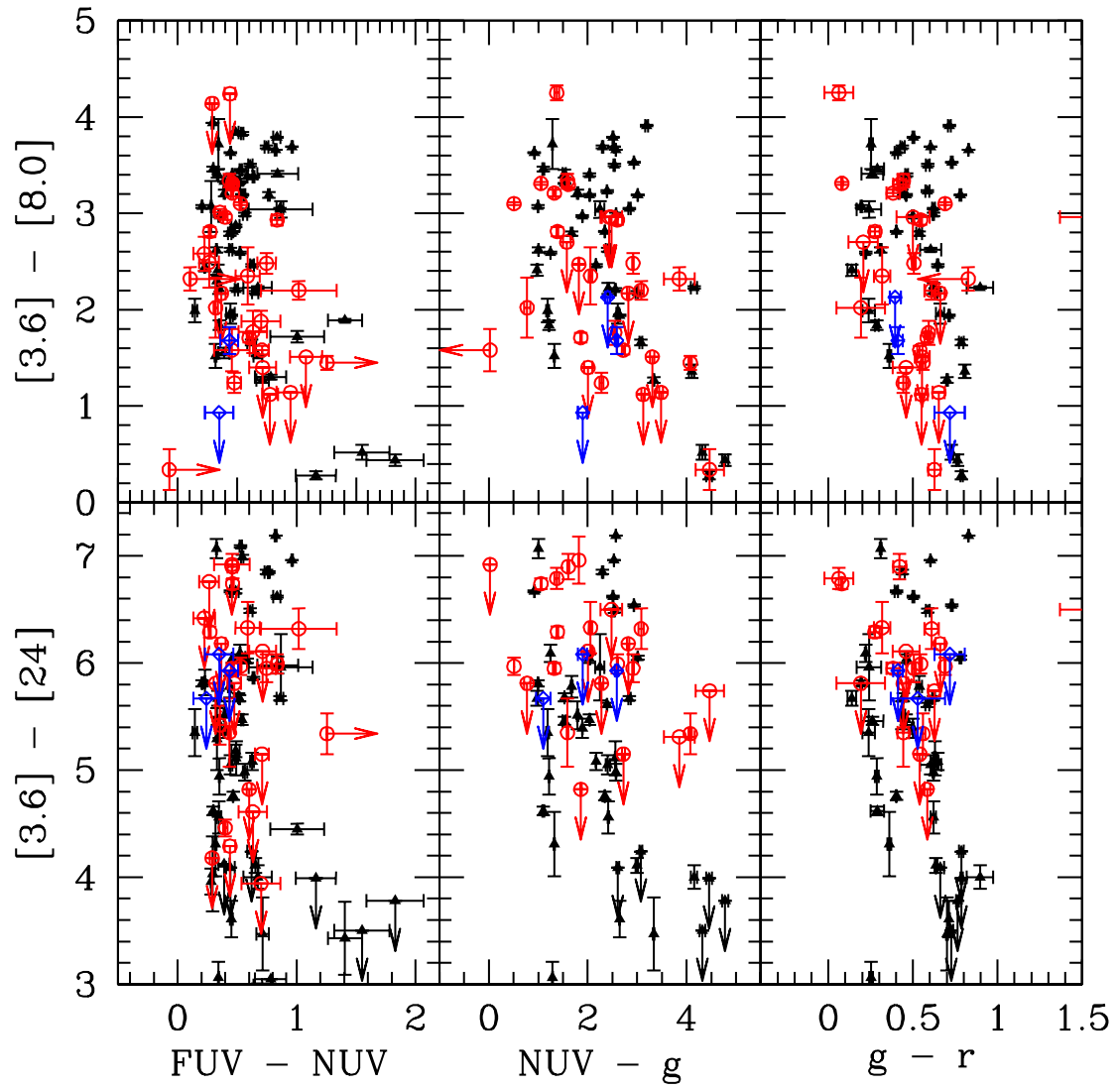


FIG. 31.— Comparison of the UV/optical colors of the SB&T disks (black filled triangles), tidal features (red open circles), and candidate TDGs (blue open diamonds) with the Spitzer $[3.6] - [24]$ and $[3.6] - [8.0]$ colors.

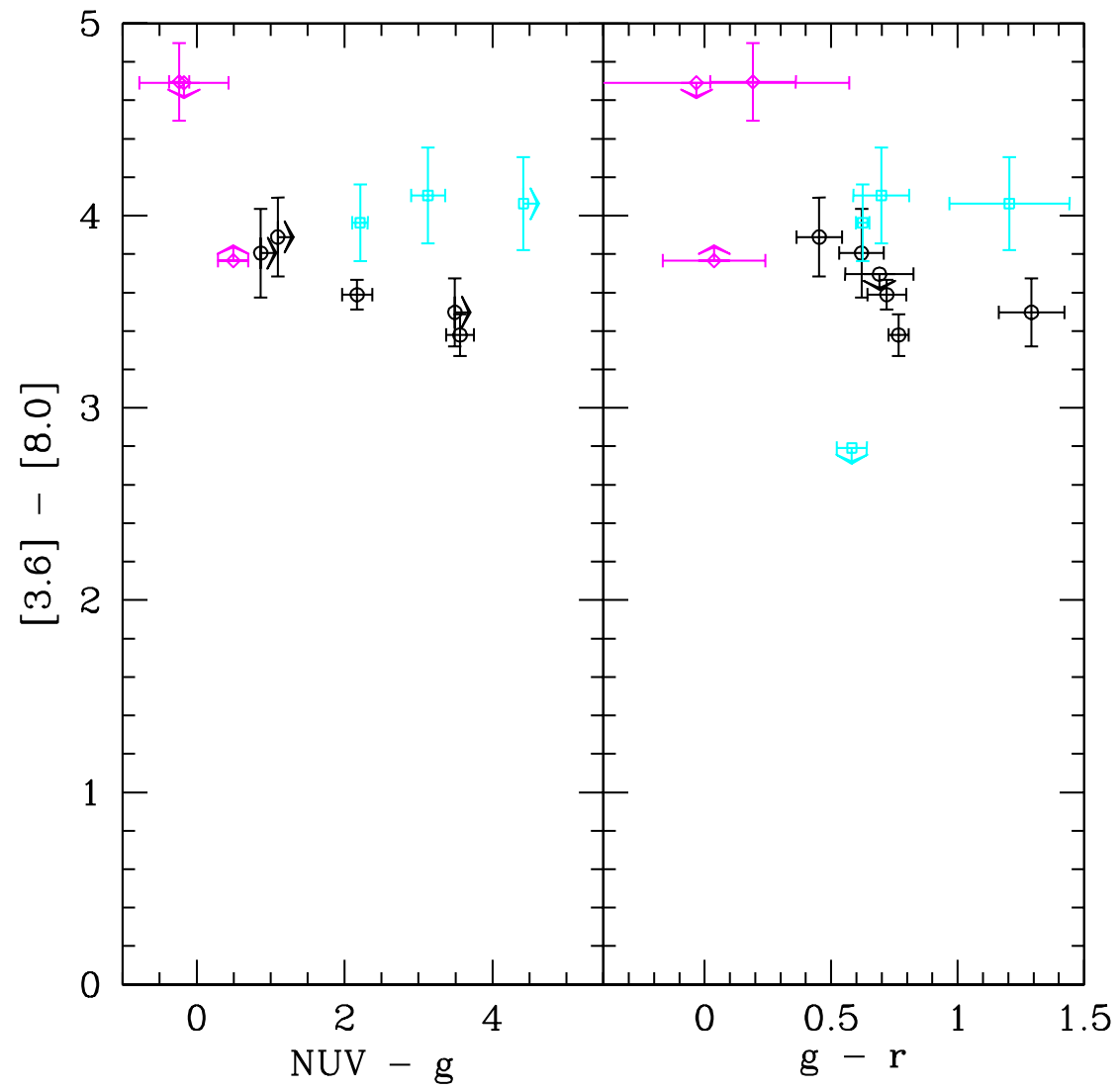


FIG. 32.— For star forming clumps in Arp 285, comparison of the $\text{NUV} - g$ and $g - r$ colors with the Spitzer $[3.6] - [8.0]$ colors. The magenta open diamonds are points from the northern tail, the cyan open circles are clumps in the NGC 2856 disk, and the black open squares are clumps in the NGC 2854 disk. Note that the axes for these plots are the same as the axes for the two upper right panels of Figure 31.

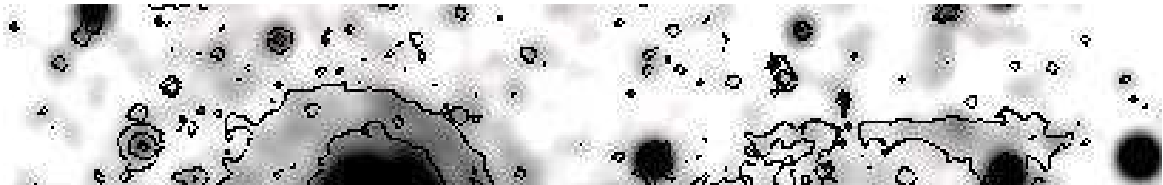


TABLE 1
THE INTERACTING GALAXY SAMPLE

System	Other Names	Distance (Mpc)	Separation (kpc)	LOG L(FIR) ^a (L _⊙)	Notes on Morphology	Nuclear Spectral Types
Arp 24	NGC 3445	29	9.6	9.5	M51-like, weak bridge	HII ^b
Arp 34	NGC 4613/4/5	67	43	10.1	Equal-mass spirals, short tails, small third galaxy	—
Arp 35	UGC 212	63	47	9.8	M51-like	—
Arp 65	NGC 90/93	70	57	9.5	Widely separated pair	—
Arp 72	NGC 5994/6	47	21	10.2	M51-like	LINER+HII ^b
Arp 82	NGC 2535/6	57	28	10.2	M51-like	HII/HII ^c , LINER/HII ^b
Arp 84	NGC 5394/5	50	28	10.7	M51-like, but bridge from smaller galaxy	HII/LINER ^{b,c}
Arp 85	M51, NGC 5194/5	6.2	8.0	9.7	M51; spiral w/ small companion, bridge	LINER/HII ^{b,c}
Arp 86	NGC 7752/3	67	40	10.7	M51-like	HII/LINER ^c
Arp 87	NGC 3808	97	29	10.8	M51-like, but near-equal mass	LINER/HII ^{b,c}
Arp 89	NGC 2648	31	22	9	M51-like	—
Arp 100	IC 18/19	85	84	—	Wide equal mass pair, long tail	—
Arp 101	UGC 10164/9	64	44	9.7	Wide equal mass pair, long tail	—
Arp 105	NGC 3561/UGC 06224	120	33	11	Equal mass spiral/elliptical pair	—
Arp 107	UGC 5984	143	46	10.1	Ring-like spiral w/ small E, bridge, short tail	Seyfert ^c
Arp 112	NGC 7805/6	66	17	9.3	Unequal mass pair	—
Arp 120	NGC 4435/8	17	22	9.4	—	—
Arp 173	UGC 09561	127	31	11	Close unequal mass pair, long tail	—
Arp 181	NGC 3212/5	129	46	10.6	Two close equal mass spirals, long tail	—
Arp 192	NGC 3303	88	2	9.6	Two close spirals, long tail	—
Arp 202	NGC 2719	44	4.7	9.75	Unequal mass pair	HII/HII ^c
Arp 242	NGC 4676	90	15	10.6	Equal mass pair, two long tails	LINER/LINER ^c , no emission ^b
Arp 244	NGC 4038/9	27	8.6	10.8	The Antennae; equal mass pair, long tails	HII/HII ^c , HII/HII+LINER ^b
Arp 245	NGC 2992/3	38	32	10.5	Equal mass separated spiral, prominent tails	—
Arp 253	UGC 173/4	29	9.8	8.7	Two close spirals, short tails	HII ^b
Arp 254	NGC 5917	28	34	9.7	Wide equal mass, long tail	—
Arp 261	—	28	7	9.3	Close spiral pair	HII ^b
Arp 269	NGC 4485/4490	8.6	9	9.8	M51-like	—
Arp 270	NGC 3395/6	27	9	9.9	Two close spirals, short tail	HII/HII ^c /LINER-HII/LINER-HII ^b
Arp 271	NGC 5426/7	40	20	10	Close equal mass spirals; bridge, no tail	HII/Seyfert ^{b,c}
Arp 280	NGC 3769	12	4.6	8.9	Unequal mass spirals, short tails	—
Arp 282	NGC 169	60	7.1	10	Close pair	no emission/HII+LINER ^c
Arp 283	NGC 2798/9	26	12	10.4	Two close spirals, tails+bridge	HII/HII ^c , HII/HII+LINER ^b
Arp 284	NGC 7714/5	34	20	10	Unequal mass pair, partial ring, tails, bridge	HII/HII ^{b,c}
Arp 285	NGC 2854/6	39	40	10	Equal mass widely separated spirals	—
Arp 290	IC 195/6	47	30	9.2	Unequal mass separated spirals	HII/LINER ^c
Arp 295	—	88	120	10.8	Wide unequal mass pair, long bridge	LINER/HII ^c
Arp 297N	NGC 5753/5	131	40	11	Spiral with small companion	HII ^c
Arp 297S	NGC 5752/4	64	35	10.2	Spiral with small companion	HII ^c
Arp 298	NGC 7469/IC5283	63	24	11.2	Disk galaxies w/ ring, disturbed companion	Seyfert/HII ^c
Arp 305	NGC 4016/4017	47	80	9.7	Wide equal mass pair	—
NGC 4567	NGC 4567	36	12	10.7	Two close spirals, no tails	—

^a Includes the IRAS flux from both galaxies in the pair.

^b Nuclear spectral type from Dahari (1985).

^c Nuclear spectral type from Keel et al. (1985).

TABLE 2
GALEX Observations

System Name ^a	Min. Obs. Date	Max. Obs. Date	Tile Name	NUV (sec)	FUV (sec)	SDSS?
Arp 24	1/31/2004	5/2/2004	LOCK_O5	85021	28080	yes
Arp 34	5/23/2007	4/3/2008	GI1_026017_Arp34	2773	2773	yes
Arp 35	9/8/2003	10/30/2007	MISDR1_29132_0390	3354	3354	
Arp 65	10/13/2004	11/2/2005	GI1_026002_Arp65	5707	3310	
Arp 72	5/20/2005	6/4/2007	GI1_026024_Arp72	4899	2609	yes
Arp 82	2/13/2005	2/25/2005	GI1_026007_Arp82	3012	1680	yes
Arp 84	4/12/2006	4/2/2008	GI1_026018_Arp84	4286	2820	yes
Arp 85	5/29/2007	5/9/2008	GI3_050006_NGC5194 NGA_M51	10136	10136	yes
Arp 86	10/2/2004	8/13/2005	GI1_026027_Arp86	3221	1679	
Arp 87	3/26/2006	3/26/2006	GI1_026015_Arp87	1595	1595	yes
Arp 89	2/18/2005	2/18/2005	GI1_026008_Arp89	1685	1685	yes
Arp 100	10/1/2004	10/1/2004	GI1_026004_Arp100	1600	1600	
Arp 101	6/17/2005	5/21/2007	GI1_026025_Arp101	5054	2326	yes
Arp 105	4/8/2005	4/8/2005	NGA_Arp105	959	—	yes
Arp 107	4/7/2005	3/25/2006	GI1_026013_Arp107	2610	1094	yes
Arp 112	9/25/2004	9/25/2004	GI1_026001_Arp112	1648	1648	yes
Arp 120	3/12/2004	4/28/2005	NGA_Virgo_MOS09	4575	1422	yes
Arp 173	5/16/2005	6/1/2007	GI1_037001_J144938p091058	11717	5111	yes
Arp 181	3/7/2005	3/7/2005	GI1_026011_Arp181	1599	1599	yes
Arp 192	2/6/2006	2/6/2006	GI1_026012_Arp192	1561	1561	yes
Arp 202	1/21/2006	1/28/2006	GI1_026009_Arp202	2693	2693	yes
Arp 242	4/8/2008	4/8/2008	GI1_077006_BDp312402	1669	1669	yes
Arp 244	2/22/2004	2/28/2004	NGA_Antennae	2365	2365	
Arp 245	1/7/2004	2/21/2005	NGA_Arp245	4283	1048	
Arp 253	3/16/2005	2/17/2006	GI1_026010_Arp253	4709	3004	
Arp 254	5/5/2006	6/3/2007	GI1_026023_Arp254	4583	2919	
Arp 261	5/4/2006	6/2/2007	GI1_026021_Arp261	3844	2157	
Arp 269	3/26/2005	3/20/2008	NGA_NGC4490	4471	3247	yes
Arp 270	3/23/2006	3/12/2007	GI1_078004_NGC3395	2660	1487	yes
Arp 271	5/4/2006	5/23/2006	GI1_009087_NGC5426	3001	1312	
Arp 280	2/26/2006	2/26/2006	GI1_026014_Arp280	1660	1660	yes
Arp 282	11/7/2004	11/4/2005	GI1_026005_Arp282	3518	1996	yes
Arp 283	2/8/2004	2/4/2007	NGA_NGC2798	4272	2798	yes
Arp 284	10/12/2004	9/13/2006	GI1_045006_Arp284	—	4736	
Arp 285	4/21/2005	4/21/2005	MISDR3_03371_0900	1419	—	yes
Arp 290	10/15/2003	10/15/2003	MISDR1_17381_0427	1669	1669	yes
Arp 295	10/5/2003	10/5/2003	NGRG_A295	1233	1233	
Arp 297	5/9/2006	5/17/2007	GI1_026020_Arp297	4639	2962	yes
Arp 298	9/4/2003	10/3/2003	NGA_NGC7469	3768	3768	
Arp 305	3/27/2006	3/27/2006	GI1_026016_Arp305	1416	1416	yes
NGC 4567	4/5/2005	4/29/2005	NGA_Virgo_MOS07	2928	—	yes

TABLE 3
OPTICAL AND UV MAGNITUDES FOR INTERACTING GALAXY SAMPLE

Arp Name	Component	Other Name	FUV (mag)	NUV (mag)	u (mag)	g (mag)	r (mag)	i (mag)	z (mag)
Arp 24	E	UGC 6021	17.89 ± 0.01	17.57 ± 0.00	17.24 ± 0.03	16.25 ± 0.01	15.88 ± 0.01	15.75 ± 0.02	15.80 ± 0.06
Arp 24	MAIN	NGC 3445	13.89 ± 0.00	13.69 ± 0.00	13.41 ± 0.00	12.69 ± 0.00	12.49 ± 0.00	12.40 ± 0.01	12.38 ± 0.02
Arp 34	NE	NGC 4615	16.41 ± 0.00	15.90 ± 0.00	15.32 ± 0.03	14.37 ± 0.00	13.93 ± 0.00	13.68 ± 0.00	13.49 ± 0.01
Arp 34	NE E TAIL	NGC 4615 EAST TAIL	16.93 ± 0.01	16.46 ± 0.00	16.28 ± 0.02	15.41 ± 0.00	15.33 ± 0.00	15.12 ± 0.01	14.87 ± 0.02
Arp 34	NE W TAIL	NGC 4615 WEST TAIL	16.97 ± 0.01	16.44 ± 0.00	16.64 ± 0.02	15.93 ± 0.00	15.24 ± 0.00	15.09 ± 0.00	15.10 ± 0.02
Arp 34	NW SMALL	NGC 4613	18.02 ± 0.02	17.39 ± 0.00	16.57 ± 0.05	15.22 ± 0.00	14.57 ± 0.00	14.26 ± 0.00	14.01 ± 0.01
Arp 34	S	NGC 4614	17.89 ± 0.05	17.17 ± 0.01	15.52 ± 0.09	13.84 ± 0.00	13.13 ± 0.00	12.77 ± 0.01	12.51 ± 0.01
Arp 35	BRIDGE	UGC 212 BRIDGE	18.01 ± 0.01	17.83 ± 0.01	—	—	—	—	—
Arp 35	N	UGC 212	15.90 ± 0.00	15.61 ± 0.00	—	—	—	—	—
Arp 35	N TAIL	UGC 212 NORTH TAIL	18.13 ± 0.02	17.95 ± 0.02	—	—	—	—	—
Arp 35	S	UGC 212notes01	18.04 ± 0.01	17.73 ± 0.01	—	—	—	—	—
Arp 35	S TAIL	UGC 212notes01 SOUTH TAIL	21.26 ± 0.04	21.16 ± 0.05	—	—	—	—	—
Arp 65	E	NGC 93	18.69 ± 0.13	17.91 ± 0.04	—	—	—	—	—
Arp 65	N TAIL	NGC 90 TAIL	19.24 ± 0.07	18.97 ± 0.04	—	—	—	—	—
Arp 65	S TAIL	NGC 90 TAIL	18.77 ± 0.08	18.54 ± 0.04	—	—	—	—	—
Arp 65	W	NGC 90	17.59 ± 0.04	17.20 ± 0.02	—	—	—	—	—
Arp 72	BRIDGE	NGC 5994/6 BRIDGE	16.54 ± 0.01	16.08 ± 0.01	15.96 ± 0.08	14.76 ± 0.03	14.38 ± 0.03	14.21 ± 0.04	14.33 ± 0.08
Arp 72	E	NGC 5996	14.40 ± 0.00	13.95 ± 0.00	13.82 ± 0.01	13.03 ± 0.01	12.63 ± 0.01	12.54 ± 0.01	12.51 ± 0.02
Arp 72	E TAIL	NGC 5996 TAIL	15.94 ± 0.01	15.67 ± 0.00	15.37 ± 0.05	14.28 ± 0.02	14.01 ± 0.02	13.95 ± 0.04	14.07 ± 0.06
Arp 72	W	NGC 5994	16.43 ± 0.00	16.10 ± 0.00	16.01 ± 0.04	15.12 ± 0.01	14.98 ± 0.02	14.89 ± 0.03	14.92 ± 0.05
Arp 82	BRIDGE	NGC 2535/6 BRIDGE	17.33 ± 0.01	16.90 ± 0.01	16.34 ± 0.08	15.25 ± 0.02	14.82 ± 0.03	14.66 ± 0.05	14.77 ± 0.05
Arp 82	E ARC	NGC 2535/6 EAST ARC	17.98 ± 0.03	17.63 ± 0.02	16.54 ± 0.16	14.75 ± 0.02	14.08 ± 0.02	13.94 ± 0.04	13.60 ± 0.03
Arp 82	N	NGC 2535	15.17 ± 0.00	14.71 ± 0.00	13.76 ± 0.02	12.65 ± 0.00	12.20 ± 0.01	11.95 ± 0.01	11.81 ± 0.01
Arp 82	N TAIL	NGC 2535 NORTH TAIL	17.50 ± 0.05	17.05 ± 0.03	>16.09	15.89 ± 0.13	15.28 ± 0.19	15.05 ± 0.33	>15.19
Arp 82	S	NGC 2536	16.49 ± 0.01	16.10 ± 0.00	15.39 ± 0.05	14.30 ± 0.01	13.87 ± 0.02	13.65 ± 0.03	13.60 ± 0.02
Arp 84	BRIDGE	NGC 5394/5 BRIDGE	18.84 ± 0.04	18.00 ± 0.01	16.94 ± 0.04	15.40 ± 0.01	14.86 ± 0.01	14.58 ± 0.01	14.66 ± 0.06
Arp 84	N	NGC 5394	17.37 ± 0.01	16.40 ± 0.00	15.11 ± 0.01	13.88 ± 0.00	13.27 ± 0.00	12.96 ± 0.00	12.70 ± 0.01
Arp 84	N TAIL	NGC 5394 TAIL	18.76 ± 0.08	18.02 ± 0.01	16.89 ± 0.06	15.10 ± 0.01	14.59 ± 0.01	14.37 ± 0.01	14.49 ± 0.10
Arp 84	S	NGC 5395	15.15 ± 0.02	14.59 ± 0.00	13.46 ± 0.01	12.01 ± 0.00	11.39 ± 0.00	11.05 ± 0.00	10.88 ± 0.02
Arp 84	S N TAIL	NGC 5395 N TAIL	20.27 ± 0.10	19.68 ± 0.03	>19.26	17.62 ± 0.03	17.30 ± 0.04	16.90 ± 0.05	>16.81
Arp 85	BRIDGE	NGC 5194/5 BRIDGE	14.78 ± 0.02	14.38 ± 0.00	—	—	—	—	—
Arp 85	N	NGC 5195	15.71 ± 0.23	14.70 ± 0.02	—	—	—	—	—
Arp 85	S	NGC 5194	11.55 ± 0.01	10.92 ± 0.00	—	—	—	—	—
Arp 86	BRIDGE	NGC 7752/3 BRIDGE	17.77 ± 0.04	17.41 ± 0.02	—	—	—	—	—
Arp 86	N	NGC 7753	15.56 ± 0.03	15.07 ± 0.01	—	—	—	—	—
Arp 86	S	NGC 7752	16.81 ± 0.02	16.32 ± 0.01	—	—	—	—	—
Arp 87	BRIDGE	NGC 3808 BRIDGE	18.96 ± 0.03	18.30 ± 0.01	17.93 ± 0.08	16.45 ± 0.01	16.21 ± 0.01	15.92 ± 0.01	15.90 ± 0.05
Arp 87	N	NGC 3808B	18.08 ± 0.03	17.25 ± 0.01	16.09 ± 0.03	14.74 ± 0.01	14.23 ± 0.00	13.93 ± 0.00	13.80 ± 0.01
Arp 87	S	NGC 3808A	16.63 ± 0.01	16.09 ± 0.00	15.28 ± 0.02	14.05 ± 0.00	13.59 ± 0.00	13.34 ± 0.00	13.19 ± 0.01
Arp 87	SMALL N	—	22.00 ± 0.26	21.13 ± 0.07	>19.95	18.89 ± 0.05	18.65 ± 0.05	18.12 ± 0.05	>18.40
Arp 87	S TAIL	NGC 3808A TAIL	20.40 ± 0.14	19.37 ± 0.03	>19.67	18.21 ± 0.04	17.65 ± 0.02	17.40 ± 0.04	17.94 ± 0.23
Arp 89	E	KPG 168	17.25 ± 0.01	16.82 ± 0.01	16.29 ± 0.06	15.14 ± 0.01	14.60 ± 0.01	14.34 ± 0.02	14.25 ± 0.03
Arp 89	E TAIL	KPG 168 EAST TAIL	20.10 ± 0.10	19.38 ± 0.05	>18.46	17.37 ± 0.06	16.92 ± 0.05	16.57 ± 0.07	16.65 ± 0.17
Arp 89	W	NGC 2648	18.08 ± 0.23	16.53 ± 0.06	14.16 ± 0.08	12.21 ± 0.01	11.48 ± 0.01	11.06 ± 0.01	10.86 ± 0.01
Arp 100	N	IC 18	19.69 ± 0.10	18.77 ± 0.03	—	—	—	—	—
Arp 100	N TAIL	IC 18 NORTH TAIL	19.34 ± 0.27	18.83 ± 0.11	—	—	—	—	—
Arp 100	S	IC 19	21.12 ± 0.25	19.33 ± 0.04	—	—	—	—	—
Arp 100	S TAIL	IC 18 SOUTH TAIL	20.03 ± 0.29	19.71 ± 0.14	—	—	—	—	—
Arp 101	BRIDGE	UGC 10164/9 BRIDGE	>18.45	18.92 ± 0.15	17.87 ± 0.33	15.33 ± 0.03	14.93 ± 0.03	14.44 ± 0.02	14.83 ± 0.05
Arp 101	N	UGC 10169	18.73 ± 0.28	17.41 ± 0.03	15.49 ± 0.03	13.89 ± 0.01	13.45 ± 0.01	13.12 ± 0.01	12.87 ± 0.01
Arp 101	N TAIL	UGC 10169 NORTH TAIL	>17.85	18.81 ± 0.22	>17.38	16.07 ± 0.10	15.45 ± 0.08	15.17 ± 0.07	15.41 ± 0.15
Arp 101	S	UGC 10164	>18.44	17.90 ± 0.05	15.74 ± 0.15	14.13 ± 0.02	13.57 ± 0.02	13.27 ± 0.02	13.18 ± 0.02
Arp 105	E TAIL	VV 237d	—	19.26 ± 0.05	>18.93	17.68 ± 0.05	17.47 ± 0.07	17.03 ± 0.08	>17.02
Arp 105	N	NGC 3561A	—	18.04 ± 0.03	16.49 ± 0.05	14.85 ± 0.01	14.13 ± 0.01	13.73 ± 0.01	13.56 ± 0.02
Arp 105	N TAIL	NGC 3561A NORTH TAIL	—	18.55 ± 0.13	>17.20	16.11 ± 0.07	15.61 ± 0.07	15.28 ± 0.09	>15.16
Arp 105	S	NGC 3561	—	18.45 ± 0.06	16.30 ± 0.05	14.35 ± 0.01	13.54 ± 0.00	13.13 ± 0.01	12.94 ± 0.02
Arp 105	S TAIL	NGC 3561 SOUTH TAIL	—	18.52 ± 0.03	17.59 ± 0.09	15.98 ± 0.01	15.38 ± 0.01	15.01 ± 0.01	15.10 ± 0.05
Arp 105	TDG	—	—	18.82 ± 0.04	18.33 ± 0.20	16.42 ± 0.02	16.02 ± 0.02	15.83 ± 0.04	16.35 ± 0.19
Arp 107	BRIDGE	UGC 5984 BRIDGE	20.26 ± 0.05	19.55 ± 0.03	>19.03	16.83 ± 0.01	16.28 ± 0.01	15.92 ± 0.03	15.89 ± 0.14
Arp 107	N	UGC 5984N	20.61 ± 0.16	19.45 ± 0.06	17.14 ± 0.12	14.99 ± 0.01	14.21 ± 0.00	13.81 ± 0.01	13.60 ± 0.05
Arp 107	N TAIL	UGC 5984N TAIL	>21.63	21.70 ± 0.28	>18.55	17.23 ± 0.03	16.60 ± 0.02	16.14 ± 0.06	16.19 ± 0.31
Arp 107	S	UGC 5984S	17.09 ± 0.01	16.60 ± 0.01	15.91 ± 0.08	14.04 ± 0.01	13.41 ± 0.00	13.07 ± 0.01	12.91 ± 0.06
Arp 107	W TAIL	UGC 5984S TAIL	20.13 ± 0.05	19.66 ± 0.03	>19.06	17.38 ± 0.02	16.93 ± 0.02	16.71 ± 0.06	16.69 ± 0.29
Arp 112	N	NGC 7806	17.72 ± 0.07	17.27 ± 0.01	15.52 ± 0.05	13.90 ± 0.00	13.18 ± 0.00	12.77 ± 0.01	12.51 ± 0.00
Arp 112	N TAIL	NGC 7806 NORTH TAIL	>19.61	19.61 ± 0.06	>17.93	16.80 ± 0.02	16.12 ± 0.03	15.74 ± 0.05	15.78 ± 0.05
Arp 112	S	NGC 7805	>19.76	19.21 ± 0.03	15.98 ± 0.04	14.09 ± 0.00	13.28 ± 0.00	12.85 ± 0.00	12.55 ± 0.00
Arp 112	TDG	KUG 2359+311	19.62 ± 0.29	18.98 ± 0.03	17.96 ± 0.29	16.20 ± 0.01	15.66 ± 0.02	15.34 ± 0.04	15.29 ± 0.03

TABLE 3 — *Continued*

Arp Name	Component	Other Name	UUV (mag)	NUV (mag)	u (mag)	g (mag)	r (mag)	i (mag)	z (mag)
Arp 120	BRIDGE	NGC 4435/8 BRIDGE	18.70 ± 0.12	17.75 ± 0.02	16.48 ± 0.23	14.26 ± 0.03	13.61 ± 0.02	13.27 ± 0.02	13.17 ± 0.05
Arp 120	N	NGC 4435	17.96 ± 0.14	16.02 ± 0.01	13.09 ± 0.02	11.30 ± 0.00	10.54 ± 0.00	10.13 ± 0.00	9.92 ± 0.01
Arp 120	N TAIL	NGC 4438 NORTH TAIL	17.00 ± 0.07	16.23 ± 0.02	14.99 ± 0.16	13.11 ± 0.03	12.56 ± 0.02	12.21 ± 0.02	12.08 ± 0.05
Arp 120	S	NGC 4438	15.51 ± 0.02	14.68 ± 0.00	12.77 ± 0.03	10.97 ± 0.00	10.20 ± 0.00	9.76 ± 0.00	9.55 ± 0.01
Arp 120	S TAIL	NGC 4438 SOUTH TAIL	18.82 ± 0.13	17.74 ± 0.02	16.37 ± 0.21	14.43 ± 0.03	13.88 ± 0.03	13.58 ± 0.03	13.48 ± 0.06
Arp 120	W TAIL	NGC 4438 WEST TAIL	19.00 ± 0.18	19.03 ± 0.09	>16.50	>16.53	>16.22	>15.99	>14.94
Arp 173	BRIDGE	UGC 9561	21.54 ± 0.25	20.64 ± 0.08	>18.90	18.10 ± 0.06	17.46 ± 0.08	16.86 ± 0.07	>17.00
Arp 173	N	UGC 9561notes01	19.54 ± 0.11	17.91 ± 0.02	16.22 ± 0.05	14.46 ± 0.00	13.83 ± 0.01	13.44 ± 0.01	13.22 ± 0.02
Arp 173	S	UGC 9561	19.60 ± 0.04	18.52 ± 0.01	17.36 ± 0.07	15.67 ± 0.01	15.06 ± 0.01	14.70 ± 0.01	14.51 ± 0.03
Arp 173	S TAIL	UGC 9561	21.49 ± 0.29	19.95 ± 0.05	>18.64	17.44 ± 0.04	16.95 ± 0.06	16.59 ± 0.07	>16.78
Arp 181	E	NGC 3215	17.24 ± 0.02	16.59 ± 0.02	15.45 ± 0.06	13.60 ± 0.01	12.96 ± 0.00	12.60 ± 0.01	12.45 ± 0.02
Arp 181	FAR WEST		18.47 ± 0.01	18.32 ± 0.02	18.36 ± 0.16	17.13 ± 0.02	16.89 ± 0.03	16.76 ± 0.05	17.53 ± 0.32
Arp 181	W	NGC 3212	17.85 ± 0.02	16.99 ± 0.02	15.95 ± 0.07	14.14 ± 0.01	13.52 ± 0.01	13.15 ± 0.01	12.98 ± 0.02
Arp 181	W TAIL	NGC 3212 TAIL	19.81 ± 0.10	18.84 ± 0.09	16.78 ± 0.12	14.58 ± 0.01	14.26 ± 0.01	13.97 ± 0.01	13.87 ± 0.04
Arp 181	TDG		20.73 ± 0.07	20.49 ± 0.08	>19.40	19.39 ± 0.12	18.86 ± 0.11	18.91 ± 0.23	>17.82
Arp 192	N	NGC 3303NED01	20.04 ± 0.12	18.89 ± 0.03	17.21 ± 0.03	15.50 ± 0.00	14.62 ± 0.00	14.34 ± 0.00	14.21 ± 0.03
Arp 192	S	NGC 3303NED02	19.17 ± 0.10	18.34 ± 0.03	15.94 ± 0.02	14.12 ± 0.00	13.48 ± 0.00	13.03 ± 0.00	12.72 ± 0.01
Arp 192	TAIL	NGC 3303 TAIL	>17.85	17.82 ± 0.18	>16.78	14.55 ± 0.03	14.00 ± 0.03	13.66 ± 0.02	>13.44
Arp 202	N	NGC 2719	15.88 ± 0.00	15.35 ± 0.00	14.89 ± 0.01	14.10 ± 0.00	13.88 ± 0.00	13.77 ± 0.01	13.72 ± 0.02
Arp 202	S	NGC 2719A	15.48 ± 0.00	15.16 ± 0.00	14.74 ± 0.01	14.15 ± 0.00	13.85 ± 0.00	13.91 ± 0.01	13.90 ± 0.03
Arp 202	W TAIL	ARP 202 WEST TAIL	21.13 ± 0.14	20.67 ± 0.05	>19.81	>20.64	>20.09	>19.05	>18.00
Arp 202	TDG		19.60 ± 0.03	19.61 ± 0.01	20.21 ± 0.31	20.07 ± 0.12	19.86 ± 0.17	>19.36	>18.28
Arp 242	BRIDGE	NGC 4676 BRIDGE	20.50 ± 0.05	19.66 ± 0.02	18.23 ± 0.08	16.63 ± 0.01	15.84 ± 0.00	15.53 ± 0.01	15.41 ± 0.02
Arp 242	N	NGC 4676A	18.37 ± 0.02	17.83 ± 0.01	16.40 ± 0.05	14.82 ± 0.01	14.03 ± 0.00	13.62 ± 0.01	13.34 ± 0.01
Arp 242	N TAIL	NGC 4676A TAIL	18.52 ± 0.03	18.06 ± 0.01	17.20 ± 0.11	15.66 ± 0.01	15.23 ± 0.01	14.90 ± 0.02	14.75 ± 0.04
Arp 242	N TDG		19.66 ± 0.07	19.22 ± 0.02	18.37 ± 0.27	16.64 ± 0.03	16.23 ± 0.01	15.82 ± 0.04	15.74 ± 0.09
Arp 242	S	NGC 4676B	17.49 ± 0.01	17.04 ± 0.00	16.00 ± 0.04	14.39 ± 0.00	13.68 ± 0.00	13.31 ± 0.00	13.04 ± 0.01
Arp 242	S TAIL	NGC 4676B TAIL	18.73 ± 0.07	18.23 ± 0.02	>17.42	15.76 ± 0.03	15.22 ± 0.01	14.94 ± 0.04	14.69 ± 0.08
Arp 242	S TDG		20.24 ± 0.11	19.89 ± 0.04	>18.44	18.00 ± 0.08	17.28 ± 0.03	17.01 ± 0.10	16.87 ± 0.23
Arp 244	N	NGC 4038	12.93 ± 0.00	12.35 ± 0.00	—	—	—	—	—
Arp 244	N TAIL	NGC 4038 TAIL	19.10 ± 0.11	18.28 ± 0.05	—	—	—	—	—
Arp 244	S	NGC 4039	15.19 ± 0.01	14.42 ± 0.00	—	—	—	—	—
Arp 244	S TAIL	NGC 4039 TAIL	17.71 ± 0.11	16.67 ± 0.04	—	—	—	—	—
Arp 244	TDG		17.29 ± 0.09	16.73 ± 0.05	—	—	—	—	—
Arp 245	BRIDGE	NGC 2992/3 BRIDGE	17.08 ± 0.11	16.45 ± 0.04	—	—	—	—	—
Arp 245	N	NGC 2992	16.00 ± 0.03	15.32 ± 0.01	—	—	—	—	—
Arp 245	N TAIL	NGC 2992 NORTH TAIL	17.81 ± 0.16	17.11 ± 0.05	—	—	—	—	—
Arp 245	S	NGC 2993	13.51 ± 0.01	13.10 ± 0.00	—	—	—	—	—
Arp 245	SE TAIL	NGC 2993 SOUTHEAST TAIL	16.98 ± 0.16	16.48 ± 0.06	—	—	—	—	—
Arp 245	TDG		17.68 ± 0.04	17.19 ± 0.01	—	—	—	—	—
Arp 253	E	UGCA 174	17.07 ± 0.01	16.74 ± 0.00	—	—	—	—	—
Arp 253	W	UGCA 173	15.95 ± 0.00	15.72 ± 0.00	—	—	—	—	—
Arp 254	BRIDGE	ARP 254 BRIDGE	>17.80	17.64 ± 0.12	—	—	—	—	—
Arp 254	N	NGC 5917	14.47 ± 0.01	14.15 ± 0.01	—	—	—	—	—
Arp 254	S	MCG -01-39-003	16.24 ± 0.03	15.72 ± 0.01	—	—	—	—	—
Arp 254	S TAIL	MCG -01-39-003 SOUTH TAIL	19.01 ± 0.12	18.30 ± 0.03	—	—	—	—	—
Arp 261	N	Arp 261NED04	16.35 ± 0.01	16.05 ± 0.00	—	—	—	—	—
Arp 261	N SMALL	KTS 52C	17.17 ± 0.01	16.77 ± 0.00	—	—	—	—	—
Arp 261	N TAIL	Arp 261 NORTHWEST TAIL	17.17 ± 0.02	16.88 ± 0.01	—	—	—	—	—
Arp 261	S	Arp 261NED01	15.19 ± 0.00	14.91 ± 0.00	—	—	—	—	—
Arp 261	SW TAIL		18.83 ± 0.04	18.39 ± 0.02	—	—	—	—	—
Arp 269	N	NGC 4485	13.66 ± 0.00	13.32 ± 0.00	12.96 ± 0.01	12.03 ± 0.01	11.78 ± 0.01	11.65 ± 0.01	11.60 ± 0.04
Arp 269	S	NGC 4490	17.18 ± 0.01	16.93 ± 0.01	16.89 ± 0.09	15.78 ± 0.03	15.34 ± 0.04	15.16 ± 0.05	15.05 ± 0.14
Arp 270	E	NGC 3396	14.19 ± 0.00	13.85 ± 0.00	13.39 ± 0.03	12.33 ± 0.04	12.07 ± 0.05	11.90 ± 0.08	11.85 ± 0.11
Arp 270	3' from TIP		20.39 ± 0.08	20.15 ± 0.06	>18.96	>18.63	>19.30	>17.16	>17.41
Arp 270	S TAIL		>19.89	19.46 ± 0.19	>17.02	>15.83	>15.08	>14.49	>14.10
Arp 270	W	NGC 3395	13.46 ± 0.00	13.16 ± 0.00	12.90 ± 0.01	12.06 ± 0.02	11.77 ± 0.03	11.63 ± 0.05	11.63 ± 0.07
Arp 270	TDG		>20.70	20.48 ± 0.22	>17.89	17.42 ± 0.30	16.78 ± 0.08	>15.83	>16.32
Arp 271	N	NGC 5427	13.71 ± 0.00	13.19 ± 0.00	—	—	—	—	—
Arp 271	S	NGC 5426	14.52 ± 0.00	14.13 ± 0.00	—	—	—	—	—
Arp 280	E	NGC 3769A	16.31 ± 0.00	15.95 ± 0.00	15.58 ± 0.04	14.74 ± 0.01	14.45 ± 0.01	14.29 ± 0.01	14.17 ± 0.09
Arp 280	W	NGC 3769	14.01 ± 0.00	13.55 ± 0.00	12.40 ± 0.01	11.20 ± 0.00	10.80 ± 0.00	10.46 ± 0.00	10.26 ± 0.01
Arp 282	E TAIL	NGC 169 TAIL	>19.49	19.39 ± 0.09	>17.17	15.53 ± 0.30	>14.70	>14.21	14.85 ± 0.36
Arp 282	N	NGC 169	18.47 ± 0.12	17.80 ± 0.02	15.53 ± 0.07	13.65 ± 0.06	12.75 ± 0.05	12.19 ± 0.05	11.80 ± 0.02
Arp 282	S	NGC 169A	17.35 ± 0.01	16.90 ± 0.00	15.75 ± 0.03	14.50 ± 0.04	13.89 ± 0.05	13.52 ± 0.05	13.32 ± 0.03
Arp 283	BRIDGE	NGC 2798/9 BRIDGE	18.98 ± 0.04	18.52 ± 0.01	18.60 ± 0.25	16.91 ± 0.02	16.49 ± 0.03	16.35 ± 0.04	16.73 ± 0.16
Arp 283	E	NGC 2799	16.22 ± 0.01	15.87 ± 0.00	15.09 ± 0.02	13.98 ± 0.00	13.48 ± 0.01	13.26 ± 0.01	13.17 ± 0.02
Arp 283	N TAIL	NGC 2798 NORTH TAIL	>20.48	19.23 ± 0.03	17.03 ± 0.11	15.15 ± 0.01	14.59 ± 0.01	14.25 ± 0.01	14.14 ± 0.03
Arp 283	S TAIL	NGC 2798 SOUTH TAIL	20.53 ± 0.31	19.52 ± 0.05	>18.02	16.44 ± 0.02	15.82 ± 0.04	15.47 ± 0.03	15.53 ± 0.10

TABLE 3 — *Continued*

Arp Name	Component	Other Name	FUV (mag)	NUV (mag)	u (mag)	g (mag)	r (mag)	i (mag)	z (mag)
Arp 283	W	NGC 2798	16.08 ± 0.01	15.26 ± 0.00	13.85 ± 0.01	12.69 ± 0.00	11.86 ± 0.00	11.56 ± 0.00	11.34 ± 0.00
Arp 284	BRIDGE	NGC 7714/5 BRIDGE	17.34 ± 0.01	—	—	—	—	—	—
Arp 284	E	NGC 7715	17.10 ± 0.00	—	—	—	—	—	—
Arp 284	E TAIL	NGC 7715 TAIL	17.45 ± 0.01	—	—	—	—	—	—
Arp 284	W	NGC 7714	14.37 ± 0.00	—	—	—	—	—	—
Arp 284	W TAIL	NGC 7714 TAIL	15.18 ± 0.00	—	—	—	—	—	—
Arp 285	BRIDGE	NGC 2854/6 BRIDGE	—	20.46 ± 0.15	>18.31	17.99 ± 0.16	16.44 ± 0.07	15.58 ± 0.07	15.30 ± 0.06
Arp 285	N	NGC 2856	—	15.97 ± 0.01	14.47 ± 0.02	13.03 ± 0.00	12.30 ± 0.00	11.98 ± 0.01	11.79 ± 0.00
Arp 285	N TAIL	NGC 2856 TAIL	—	19.37 ± 0.02	19.44 ± 0.28	18.00 ± 0.04	17.93 ± 0.07	17.49 ± 0.15	17.98 ± 0.19
Arp 285	S	NGC 2854	—	15.80 ± 0.01	14.75 ± 0.03	13.41 ± 0.01	12.82 ± 0.01	12.49 ± 0.01	12.33 ± 0.01
Arp 285	S TAIL	NGC 2854 SOUTH TAIL	—	20.12 ± 0.13	>18.21	>18.29	>17.48	>17.14	>16.53
Arp 290	N	IC 196	17.03 ± 0.03	16.41 ± 0.02	15.25 ± 0.07	13.33 ± 0.01	12.54 ± 0.01	12.13 ± 0.01	11.95 ± 0.03
Arp 290	N TAIL	IC 196 TAIL	17.89 ± 0.02	17.29 ± 0.01	17.18 ± 0.07	15.42 ± 0.01	14.84 ± 0.01	14.44 ± 0.01	14.32 ± 0.04
Arp 290	S	IC 195	20.42 ± 0.23	18.59 ± 0.06	15.78 ± 0.05	13.81 ± 0.01	13.04 ± 0.01	12.62 ± 0.01	12.42 ± 0.02
Arp 295	BRIDGE	ARP 295 BRIDGE	>20.19	19.12 ± 0.14	—	—	—	—	—
Arp 295	N	ARP 295B	16.75 ± 0.01	16.21 ± 0.01	—	—	—	—	—
Arp 295	S	ARP 295A	19.75 ± 0.13	18.34 ± 0.05	—	—	—	—	—
Arp 295	S TAIL	ARP 295A TAIL	20.04 ± 0.17	19.06 ± 0.09	—	—	—	—	—
Arp 297	NE	NGC 5755	17.48 ± 0.01	16.73 ± 0.01	15.95 ± 0.05	14.43 ± 0.01	13.99 ± 0.01	13.75 ± 0.01	13.66 ± 0.05
Arp 297	NE N TAIL	NGC 5755 TAIL	18.86 ± 0.04	18.08 ± 0.02	>18.09	16.62 ± 0.06	16.37 ± 0.04	16.22 ± 0.08	>15.87
Arp 297	NW	NGC 5753	18.74 ± 0.03	18.30 ± 0.02	17.56 ± 0.13	15.69 ± 0.02	15.03 ± 0.01	14.69 ± 0.02	14.62 ± 0.07
Arp 297	SE	NGC 5754	15.96 ± 0.01	15.61 ± 0.01	14.86 ± 0.07	13.19 ± 0.01	12.57 ± 0.01	12.26 ± 0.01	12.14 ± 0.05
Arp 297	SE TAIL	NGC 5754 TAIL	20.07 ± 0.07	19.35 ± 0.04	>18.62	17.13 ± 0.06	16.66 ± 0.03	16.21 ± 0.05	>16.48
Arp 297	SW	NGC 5752	18.17 ± 0.02	17.56 ± 0.01	16.40 ± 0.04	15.03 ± 0.01	14.44 ± 0.01	14.16 ± 0.01	14.01 ± 0.04
Arp 297	W TAIL	NGC 5452 TAIL	>20.45	19.46 ± 0.12	>17.56	17.13 ± 0.16	16.55 ± 0.07	16.12 ± 0.10	>15.47
Arp 298	N	IC 5283	18.20 ± 0.16	17.36 ± 0.07	—	—	—	—	—
Arp 298	S	NGC 7469	14.57 ± 0.01	14.04 ± 0.01	—	—	—	—	—
Arp 298	W TAIL	IC 5283 TAIL	>19.37	>19.34	—	—	—	—	—
Arp 305	BRIDGE	NGC 4016/7 BRIDGE	16.89 ± 0.01	16.61 ± 0.00	16.45 ± 0.05	15.37 ± 0.02	15.10 ± 0.04	15.07 ± 0.10	15.09 ± 0.10
Arp 305	N	NGC 4016	15.40 ± 0.01	15.19 ± 0.00	15.02 ± 0.03	14.12 ± 0.01	13.80 ± 0.02	13.58 ± 0.06	13.56 ± 0.05
Arp 305	N TAIL	NGC 4016 NORTH TAIL	17.51 ± 0.03	17.27 ± 0.01	18.03 ± 0.27	16.47 ± 0.07	16.09 ± 0.11	15.85 ± 0.25	>16.00
Arp 305	S	NGC 4017	15.44 ± 0.01	15.05 ± 0.00	14.50 ± 0.02	13.44 ± 0.01	13.00 ± 0.01	12.83 ± 0.03	12.72 ± 0.02
Arp 305	S TAIL	NGC 4017 SOUTH TAIL	16.44 ± 0.07	16.14 ± 0.02	>15.94	14.89 ± 0.12	14.34 ± 0.16	>13.78	>13.90
Arp 305	TDG	—	18.16 ± 0.02	18.02 ± 0.01	>18.73	17.92 ± 0.13	17.79 ± 0.27	>16.71	>16.68
NGC 4567	N	—	—	14.13 ± 0.01	12.80 ± 0.02	11.44 ± 0.01	10.78 ± 0.01	10.47 ± 0.01	10.29 ± 0.02
NGC 4567	S	—	—	13.69 ± 0.01	12.61 ± 0.02	11.15 ± 0.01	10.52 ± 0.01	10.14 ± 0.01	9.89 ± 0.02

This figure "bsmith_fig1.jpg" is available in "jpg" format from:

<http://arxiv.org/ps/1001.0989v1>

This figure "bsmith_fig2.jpg" is available in "jpg" format from:

<http://arxiv.org/ps/1001.0989v1>

This figure "bsmith_fig3.jpg" is available in "jpg" format from:

<http://arxiv.org/ps/1001.0989v1>

This figure "bsmith_fig4.jpg" is available in "jpg" format from:

<http://arxiv.org/ps/1001.0989v1>

This figure "bsmith_fig5.jpg" is available in "jpg" format from:

<http://arxiv.org/ps/1001.0989v1>

This figure "bsmith_fig6.jpg" is available in "jpg" format from:

<http://arxiv.org/ps/1001.0989v1>

This figure "bsmith_fig7.jpg" is available in "jpg" format from:

<http://arxiv.org/ps/1001.0989v1>

This figure "bsmith_fig8.jpg" is available in "jpg" format from:

<http://arxiv.org/ps/1001.0989v1>

This figure "bsmith_fig9.jpg" is available in "jpg" format from:

<http://arxiv.org/ps/1001.0989v1>

This figure "bsmith_fig10.jpg" is available in "jpg" format from:

<http://arxiv.org/ps/1001.0989v1>

This figure "bsmith_fig11.jpg" is available in "jpg" format from:

<http://arxiv.org/ps/1001.0989v1>

This figure "bsmith_fig12.jpg" is available in "jpg" format from:

<http://arxiv.org/ps/1001.0989v1>

This figure "bsmith_fig13.jpg" is available in "jpg" format from:

<http://arxiv.org/ps/1001.0989v1>

This figure "bsmith_fig14.jpg" is available in "jpg" format from:

<http://arxiv.org/ps/1001.0989v1>

This figure "bsmith_fig15.jpg" is available in "jpg" format from:

<http://arxiv.org/ps/1001.0989v1>

This figure "bsmith_fig16.jpg" is available in "jpg" format from:

<http://arxiv.org/ps/1001.0989v1>

This figure "bsmith_fig17.jpg" is available in "jpg" format from:

<http://arxiv.org/ps/1001.0989v1>

This figure "bsmith_fig18.jpg" is available in "jpg" format from:

<http://arxiv.org/ps/1001.0989v1>